Journal of Pharmaceutical Analysis 14 (2024) 100934

Contents lists available at ScienceDirect

Journal of Pharmaceutical Analysis

journal homepage: www.elsevier.com/locate/jpa

Original article

Baicalin reduces chronic stress-induced breast cancer metastasis via directly targeting β2-adrenergic receptor

Qi Jia [a, 1], Yinyin Zhou [a, 1], Li Song [a, 1], Ximeng Shi [d, 1], Xuan Jiang [a], Ruizhi Tao [a], Aiyun Wang [a, b, c], Yuanyuan Wu [a], Zhonghong Wei [a], Yinan Zhang [d, **], Xiaoman Li [a, *], Yin Lu [a, b, c, ***]

[a] Jiangsu Key Laboratory for Pharmacology and Safety Evaluation of Chinese Materia Medica, School of Pharmacy, Nanjing University of Chinese Medicine, Nanjing, 210023, China
[b] Jiangsu Joint International Research Laboratory of Chinese Medicine and Regenerative Medicine, Nanjing University of Chinese Medicine, Nanjing, 210023, China
[c] Jiangsu Collaborative Innovation Center of Traditional Chinese Medicine (TCM) Prevention and Treatment of Tumor, Nanjing University of Chinese Medicine, Nanjing, 210023, China
[d] Jiangsu Key Laboratory for Functional Substances of Chinese Medicine, School of Pharmacy, Nanjing University of Chinese Medicine, Nanjing, 210023, China

ARTICLE INFO

Article history:
Received 8 September 2023
Received in revised form
13 December 2023
Accepted 2 January 2024
Available online 4 January 2024

Keywords:
Baicalin
Chronic stress
Breast cancer metastasis
β2-adrenergic receptor
Epithelial-mesenchymal transition

ABSTRACT

Recent studies have shown that stress can substantially facilitate breast cancer metastasis, which can be reduced by nonselective β1/β2-adrenergic receptor (β1/β2-AR) blocker. However, several side effects were identified. Thus, it is extremely warranted to explore more effective and better-tolerated β2-AR blocker. Currently, we demonstrated that baicalin (BA), a major bioactive component of *Scutellaria baicalensis* Georgi, could significantly attenuate stress hormones especially epinephrine (Epi)-induced breast cancer cell migration and invasion *in vitro*. Mechanistically, we identified that β2-AR was a direct target of BA via the drug affinity responsive target stability (DARTS) combined with mass spectrum assay, and BA photoaffinity probe with pull-down assay, which was further confirmed by a couple of biophysical and biochemical assays. Furthermore, we demonstrated that BA could directly bind to the Phe-193 and Phe-289 of β2-AR, subsequently inhibit cyclic adenosine monophosphate-protein kinase A-focal adhesion kinase (cAMP-PKA-FAK) pathway, and thus impede epithelial-mesenchymal transition (EMT), thereby hindering the metastatic progression of the chronic stress coupled with syngeneic and xenograft *in vivo* orthotopic and tail vein mouse model. These findings firstly identify BA as a potential β2-AR inhibitor in the treatment of stress-induced breast cancer metastasis.

1. Introduction

Breast cancer continues to be the primary cause of cancer-induced fatalities in women globally [1]. Although early diagnosis and recent targeted therapy significantly improved the survival rate of breast cancer [2,3], the average duration is approximately only three years as a result of a high rate of cancer metastasis [4]. Accumulating evidence showed that psychosocial stress is a significant biological factor underlying cancer etiology and progression mediated by excess activation of the sympathetic nervous system (SNS) releasing norepinephrine (NE) and epinephrine (Epi) and to a lesser degree by the hypothalamic-pituitary-adrenal (HPA) axis responsible for the release of stress hormones [5,6]. Pharmacologically decreasing these stress hormones or interfering their signal pathway thus becomes a prior strategy in the search of anti-metastasis drugs [7,8].

β2-adrenergic receptor (β2-AR), encoded by *ADRB2*, as a major responder to catecholamines, has been examined as a potential contributor to stress-induced cancer progression in various cancers [9,10]. Multiple pre-clinical studies have shown that β-blockers can

* Corresponding author.
** Corresponding author.
*** Corresponding author. Jiangsu Key Laboratory for Pharmacology and Safety Evaluation of Chinese Materia Medica, School of Pharmacy, Nanjing University of Chinese, Nanjing, 210023, China.
E-mail addresses: yinanzhang@njucm.edu.cn (Y. Zhang), lixm@njucm.edu.cn (X. Li), luyingreen@njucm.edu.cn (Y. Lu).
[1] These authors contributed equally to this work.

https://doi.org/10.1016/j.jpha.2024.01.002

hinder stress-induced release of NE and Epi, leading to retardation of pro-growth and pro-metastatic effects [11,12]. To this end, propranolol was recognized as a neoadjuvant therapy to enter the clinical trials primarily [11,13]. However, it was found that the non-selective role of propranolol on the β1-AR led to several side effects, such as cardiac disorders, rash, fatigue and vitiligo [14]. Therefore, further development of more effective and better-tolerated treatments is warranted.

Nature has been continuing to be a major source of medicinal products, and especially providing revolutionized structural leads in the treatment of serious diseases for millennia [15]. Our group aims to characterize active natural product and resolve their underlying mechanism in tumor vascular normalization and attenuating the stemness of cancers [16,17]. In the search of anti-metastasis materials, we noticed *Scutellaria baicalensis* Georgi has been intensively recorded to treat cancer and depression-related symptoms in a variety of traditional pharmacopeia and contemporary traditional Chinese medicine clinical practice [18,19]. As the predominant constituents in the herb, baicalin (BA) has been known to possess anti-cancer and anti-depression activities [20,21]. While these studies focused on either tumor cells or neurons independently, the effect of BA on stress-induced breast cancer metastasis has not been concerned. To address this, we herein used Epi as stress hormone *in vitro*, which was markedly upregulated in chronic unpredictable mild stress (CUMS) and chronic restraint stress (CRS) models and promoted the metastasis of breast cancer cells most significantly among other stress hormones *in vitro*. The results showed that Epi-mediated breast cancer cell migration was reduced by BA. We next identified that β2-AR is predicted to be the direct target of BA via BA photoaffinity probe assay and drug affinity responsive target stability (DARTS) assay, which was further confirmed by a couple of biophysical and biochemical assays. The mechanistic investigations highlighted BA impeded epithelial-mesenchymal transition (EMT) by β2-AR-cyclic adenosine monophosphate-protein kinase A-focal adhesion kinase (cAMP-PKA-FAK) pathway. The above effects and the underlying mechanisms of BA were also verified using syngeneic and xenograft *in vivo* orthotopic and tail vein mouse models of breast cancer combined with CUMS or CRS. These results supported the blockade of β2-AR as a strategy for reducing metastatic breast cancer.

2. Materials and methods

2.1. Cell culture and reagents

Human breast cancer cell lines (MCF-7 and MDA-MB-231) and murine mammary carcinoma cell lines (4T1 and EO771) were preserved in our laboratory and authenticated using the short tandem repeat DNA profiling method every 6 months. The cell lines were cultured in standard medium (KeyGen BioTech, Nanjing, China) recommended by the American Type Culture Collection (Manassas, VA, USA) in a humidified atmosphere with 5% CO_2 at 37 °C. Mycoplasma testing was performed every 2 weeks.

BA (Cat# S30647), Epi (Cat# B27670), and NE (Cat# S25926) were purchased from Shanghai yuanye Bio-Technology Co., Ltd (Shanghai, China), while ICI 118551 (Cat# HY-13951), cortisol (Cort, Cat# HY-N0583), salmeterol (SAL, Cat# HY-13951), a selective human β2-AR agonist, and isoprenaline (ISO, Cat# HY-B0468) were purchased from MedChemExpress (Monmouth Junction, NJ, USA).

2.2. Ethics statement

The ethical policies and procedures approved by the Ethics Committee of Nanjing University of Chinese Medicine (Approval number: 202008A015) were followed in all animal experiments.

2.3. Animal model construction and drug administration

Female BALB/c nude mice (6 weeks old) were purchased from GemPharmatech (Nanjing, China) and restrained in well-ventilated 50 mL conical tubes for 4 h per day to establish the CRS model. For the CUMS model, female BALB/c and C57BL/6J mice (6 weeks old) were subjected to various stressors, including food or water deprivation for 12 h, tail pinch for 1.5 min, cold swim at 4 °C for 5 min, vibration for 15 min, exposure to damp bedding for 24 h, 4 h of restraint, and 24 h of 45° cage tilt. The stressors were randomly applied to the mice every day to ensure the unpredictability of the stressors, and all stressors were repeated throughout the experiment. Before injecting cancer cells, the mice underwent a 7-day period of stress pre-treatment. For the breast cancer *in situ* model, MCF-7, MDA-MB-231, or MCF-7 overexpression of green fluorescent protein (GFP) and β2 adrenergic receptor (ADRB2) (MCF-7 $ADRB2^{OE}$) cells (6×10^6 cells in 100 μL phosphate buffer saline (PBS)) was introduced into the pre-cleaned 4th mammary fat pads of BALB/c nude mice, while 4T1 cells overexpressing GFP (5×10^5 cells in 50 μL PBS) were injected into the pre-cleaned 4th mammary fat pads of BALB/c mice. Eight days later, BA was administered by intragastric administration every day at 100 mg/kg and 50 mg/kg until the mice were sacrificed. For the metastatic mouse model, MDA-MB-231 cells (2×10^6 cells in 100 μL PBS) and EO771 cells overexpressing GFP (2×10^5 cells in 100 μL PBS) were intravenously injected into BALB/c nude mice and C57BL/6J mice, respectively. The mice were daily intragastrically administrated with BA at 100 mg/kg and 50 mg/kg the next day.

2.4. Measurement of neurotransmitter and stress hormone

We utilized enzyme linked immunosorbent assay (ELISA) kits (R&D Systems, Minneapolis, MN, USA) with the manufacturer's guidelines to measure the concentrations of dopamine (DA) and 5-hydroxytryptamine (5-HT) in the mouse hippocampus, as well as Epi, NE, and corticosterone in the serum. Following the collection of blood samples, the mice were euthanized and their brains were subsequently removed. The hippocampus was immediately isolated at 4 °C and homogenized in PBS (the volume depends on the tissue weight). The homogenates were then centrifuged at 5,000 *g* for 5 min to obtain the supernatant. Blood samples were centrifuged for 20 min at approximately 1,000 *g* to obtain the serum after overnight clotting at 4 °C. ELISA was carried out according to the instructions provided by the manufacturer, and the absorbance was measured at 450 nm.

2.5. cAMP quantification

Intracellular levels of cAMP were quantified colorimetrically using a cAMP ELISA kit (No. 581001, Cayman Chemical, Ann Arbor, MI, USA). Results are presented as pmol of cAMP per mL of protein.

To determine the binding mode of BA with β2-AR, MDA-MB-231 and 4T1 cells were grown to confluence in 6-well plates, and gradient concentration of Epi and SAL were added, respectively. Following a 15 min interval, each well was supplemented with 100 μM and 10 μM BA and left to incubate for 30 min. Then cAMP concentration was measured following the above steps.

2.6. Three-dimensional (3D) spheroid assay

To measure the 3D invasion of breast cancer cells, a tissue culture system was employed. The system was set up in a glass-bottom culture dish (Cat# 801002, Nest, Wuxi, China), where cancer cells were placed in a central 3D matrix which allowed cells to invade into the outer matrix. 1×10^6 cells/well were suspended in 10 μL of

culture medium containing matrigel (Cat# 354234, Corning, Corning, NY, USA) (2:1, *V/V*). 1 μL of cell suspension was added at the center of the culture dish and allowed to solidify. The outer matrix, a mixture of matrigel and cell culture medium (1:2, *V/V*), was added to cover the central matrix. After solidification, the setup was overlaid with culture medium. Cells were allowed to invade into the outer matrix for 24 h. Images of the system were acquired at 0 h and 24 h by microscope, and the invasion area was quantified.

2.7. Transwell assay

In short, the upper chamber was filled with 0.8×10^5 cells in 200 μL of serum-free medium, while the lower chamber was loaded with complete medium containing 10% fetal bovine serum (FBS; Sigma-Aldrich, St. Louis, MO, USA). The cells were then allowed to migrate for 24 h. Subsequently, they were fixed, stained with crystal violet, and counted in three random fields using an inverted microscope (× 200) (Zeiss, Oberkochen, BW, Germany).

2.8. Wound healing assay

The previous study was used as a reference to conduct the wound healing assay [22], and the gap distance was quantitatively evaluated using Image J software (Media Cybernetics, Silver Springs, MD, USA).

2.9. Construction of breast cancer cell lines stably expressing GFP or ADRB2

To establish 4T1 and EO771 cell lines stably overexpressing GFP, lentivirus infection was used with particles by Genechem (Shanghai, China) with titers above 1×10^8 TU/mL. Stable expression of GFP was confirmed through puromycin selection and observation of green fluorescence. Similarly, MCF-7 cells with stable overexpression of ADRB2 were constructed using lentivirus infection, denoted as MCF-7 ADRB2^{OE}, with lentiviral particles from GenePharma (Shanghai, China) with titers above 1×10^8 TU/mL. Western blotting analysis confirmed a significant increase in β2-AR expression. MCF-7 ADRB2^{OE} cells were further infected with lentiviral particles expressing GFP to establish MCF-7 ADRB2^{OE} overexpressing GFP.

2.10. Construction of MDA-MB-231 cells overexpressing F193A- and F289A-β2-AR

MDA-MB-231 cells with ADRB2 knockout (MDA-MB-231 ADRB2^{KO}) were used to establish MDA-MB-231 overexpressing F193A- and F289A-β2-AR using plasmid pEGFP-N-ADRB2 expressing the amino acid phenylalanine at position 193 and 289 of β2-AR, which was simultaneously mutated to alanine. Lipofectamine®2000 (Cat# 11668, Invitrogen, Carlsbad, CA, USA) was utilized to transfect the plasmid into MDA-MB-231 ADRB2^{KO} cells. The resulting cells were named MDA-MB-231^{Mu}, and quantitative polymerase chain reaction (qPCR) and Western blotting were employed to verify the knockdown efficiency of ADRB2. Fluorescence microscopy was used to confirm the re-expression of F193A- and F289A-β2-AR.

2.11. DARTS

To simulate a stress environment, MDA-MB-231 or MDA-MB-231^{Mu} cells were incubated with Epi (10 μM) for 15 min followed by DARTS [23]. The cells were lysed with M-PER lysis buffer (Cat# 78503, Thermo Fisher, Waltham, MA, USA) containing protease (Cat# ST506, Beyotime, Beijing, China) and phosphatase inhibitors (Cat# P1082, Beyotime). The lysates were subjected to centrifugation at 12,000 rpm for 15 min at 4 °C, resulting in the collection of the supernatant. Subsequently, the supernatant was divided into two parts and incubated with either BA (500 μM) or dimethyl sulfoxide (DMSO) (equal volume) at room temperature for 20–30 min. Each lysate was then equally divided into six parts, and proteolysis was performed without or with different ratios of pronase (Cat# 10165921001, Roche, Basel, Switzerland) to protein (1 μg pronase to 100 μg protein at the ratio of 1:100, 1:300, 1:1,000, 1:3,000, and 1:10,000 (*m/m*)) for 30 min at room temperature. The reaction was stopped by adding loading buffer and boiling immediately. The resulting samples were loaded onto 10% sodium dodecyl sulfate-polyacrylamide gel electrophoresis (SDS-PAGE) for either gel staining or Western blotting.

To identify the enriched proteins, differential protein bands on the Coomassie brilliant blue-stained SDS-PAGE gel were excised and subjected to liquid chromatography tandem-mass spectrometry (LC-MS/MS) analysis [24] which was conducted on a LTQ Orbitrap Velos Pro mass spectrometer (Thermo Finnigan, Waltham, MA, USA) coupled with an EASY-nLC1000 Nano-HPLC system, following a published protocol [25].

2.12. Screening of BA targets

To identify potential targets of BA in inhibiting chronic stress-induced breast cancer metastasis, we used DARTS followed by filtering the genes associated with breast cancer metastasis and Epi using OMIM (https://omim.org/) and GeneCards (https://www.genecards.org) databases. The targets were sorted out based on a screening criterion of 2 times the median of the relevance value in the GeneCards database, and then integrated with the targets in the OMIM database. Statistical data detected by LC-MS/MS were used to screen out proteins with a difference of more than 1.2 between the BA and solvent control group to identify BA targets. The common targets of BA, breast cancer metastasis and Epi were then selected, and the binding affinity of BA to target protein was verified by molecular docking using AutoDockTools (Alabaster, AL, USA).

2.13. Cellular thermal shift assay (CETSA)

Lysates from MDA-MB-231 cells or MDA-MB-231^{Mu} cells incubated with Epi (10 μM) for 15 min were collected and subjected to CETSA [26]. Lysates (5 mg/mL) were incubated with BA (500 μM) or DMSO at a range of temperatures (42–64 °C for MDA-MB-231 cells and 42–67 °C for MDA-MB-231^{Mu} cells) for 3 min. Following centrifugation, the supernatant was collected, mixed with loading buffer, and boiled immediately. Western blotting was then used to analyze the samples.

2.14. Micro scale thermophoresis (MST)

To confirm the interaction between BA and β2-AR, purified β2-AR protein was used in MST. The protein was provided by GZL Bioscience (Hangzhou, China) via cell-free protein expression and labelled with red fluorescent dye NT-L118 (NanoTemper, Munich, Germany) as per the manufacturer's recommendation. We conducted binding assays using a Monolith NT.115 instrument (NanoTemper). To improve K_d determination accuracy, labelled-β2-AR protein was kept at a minimum concentration of 20 nM and titrated with different concentrations of BA ranging from 38.1 nM to 12.5 mM.

2.15. Bio-layer interferometry (BLI)

Biotinylated of β2-AR was immobilized on the super streptavidin (SSA) sensors using 20 μg/mL provided and analyzed using BLI technique on a ForteBio Octet Red96e instrument (Pall Life Sciences, East Hills, NY, USA). 500 μM BA was applied on the BA-coated sensors, and the interaction data was background-subtracted, normalized, and analyzed using linear regression analysis with ForteBio Data Analysis 10.0.

2.16. General chemistry

^{1}H (500 MHz) and ^{13}C (125 MHz) nuclear magnetic resonance (NMR) spectra were recorded on a Bruker AV-500 device (Bruker, Karlsruher, Germany). The chemical shifts were reported in d (ppm) with the δ 7.26 signal of $CDCl_3$ and δ 3.31signal of CD_3OD (^{1}H NMR), and the δ 77.16 signal of $CDCl_3$ and δ 49.00 signal of CD_3OD (^{13}C NMR) as internal control. The following abbreviations were utilized to explain the multiplicities: s = singlet, d = doublet, t = triplet, q = quartet, and m = multiplet. high resolution-electrospray ionization-mass spectrometry (HR-ESI-MS) assays were performed by a Thermo Fisher Scientific Q Exactive Plus in the positive mode. If not specifically stated, all commercially obtainable solvents and reagents were utilized as-is without additional purification. The reaction was monitored by LC-MS/MS or analytical thin-layer chromatography (TLC) purchased from Jiangyou Chemical Co., Ltd (Yantai, China). Column chromatography on silica gel (200–300 mesh) was obtained from Haiyang Chemical Co., Ltd (Qingdao, China). Detailed information for the preparation of 2-(3-(but-3-yn-1-yl)-3H-diazirin-3-yl)ethan-1-amine [27] is shown as below.

2.17. Preparation of 2-(3-(but-3-yn-1-yl)-3H-diazirin-3-yl)ethan-1-amine (C8)

The procedure of preparation of 2-(3-(but-3-yn-1-yl)-3H-diazirin-3-yl)ethan-1-amine (**C8**) is shown in Scheme 1.

Synthesis of ethyl 3-oxohept-6-ynoate (**C1**). A stirred solution of lithium diisopropylamine (LDA) (2.0 M solution in tetrahydrofuran (THF), 50 mL) in dry THF (40 mL) was added to ethyl acetoacetate (6.5 g, 50 mmol, in 10 mL of THF) at −40 °C under an argon atmosphere. After stirring for 30 min, propargyl bromide (5.4 mL, 60 mmol) was added in one portion and the resulting solution was stirred at 0 °C for additional 3 h. The mixture was quenched with saturated aqueous NH_4Cl and extracted with ethyl acetate (EA) for twice. The combine organic layers were washed with brine, dried over Na_2SO_4, filtered, and concentrated. After purification by flash column chromatography on silica gel using petroleum ether (PE)/EA (15:1, *V/V*), the desired product **C1** (6 g, 71% yield) was obtained as a yellow liquid. The spectral data are consistent with previous publication [28]. TLC (PE/EA = 5:1, *V/V*): R_f = 0.45 [$KMnO_4$]. ^{1}H NMR (500 MHz, $CDCl_3$) δ 4.19 (q, *J* = 7.1 Hz, 2H), 3.46 (s, 2H), 2.81 (t, *J* = 7.2 Hz, 2H), 2.47 (ddd, *J* = 7.8, 6.7, 2.6 Hz, 2H), 1.95 (t, *J* = 2.7 Hz, 1H), 1.28 (t, *J* = 7.1 Hz, 3H).

Synthesis of ethyl 2-(2-(but-3-yn-1-yl)-1,3-dioxolan-2-yl)acetate (**C2**). **C1** (5.0 g, 30 mmol), ethylene glycol (3.7 g, 60 mmol), and p-toluene sulfonic acid (PTSA) (1.0 g, 6 mmol) were added to 150 mL of toluene. The reaction was equipped with a Dean-Stark apparatus (Milwaukee, WI, USA) and refluxed overnight at 130 °C. The saturated $NaHCO_3$ was used to dilute the reaction, and the resulting mixture was extracted twice with EA. The organic layers were then combined and washed with brine before being dried over Na_2SO_4. Finally, the mixture was concentrated. After purification with flash column chromatography on silica gel using PE/EA (5:1, *V/V*), the desired product **C2** (5.5 g, 91% yield) was obtained as a colorless liquid. The spectral data are consistent with previous publication [28]. TLC (PE/EA = 5:1, *V/V*): R_f = 0.3 [$KMnO_4$]. ^{1}H NMR (500 MHz, $CDCl_3$) δ 4.15 (q, *J* = 7.1 Hz, 2H), 4.02–3.94 (m, 4H), 2.65 (s, 2H), 2.32–2.26 (m, 2H), 2.14–2.09 (m, 2H), 1.92 (t, *J* = 2.7 Hz, 1H), 1.26 (t, *J* = 7.2 Hz, 3H).

Synthesis of 2-(2-(but-3-yn-1-yl)-1,3-dioxolan-2-yl)ethan-1-ol (**C3**). To a stirred suspension of $LiAlH_4$ (3.0 g, 80 mmol) in anhydrous ether (100 mL) at 0 °C was added an ethereal solution of **C2** (4.3 g, 20 mmol). After stirring for 30 min at room temperature, the reaction was quenched by adding H_2O (3 mL), 5 M NaOH (3 mL), and H_2O (10 mL). The filtered precipitates were washed twice with EA. The resulting organic solvents were combined and concentrated in vacuo, yielding the crude product. The crude product was then purified using PE/EA (2:1, *V/V*) on silica gel, resulting in the isolation of **C3** (2.4 g, 70% yield) as a colorless oil. The spectral data are consistent with previous publication [28,29]. TLC (PE/EA = 2:1, *V/V*): R_f = 0.43 [$KMnO_4$]. ^{1}H NMR (500 MHz, $CDCl_3$) δ 4.04–3.95 (m, 4H), 3.80–3.72 (m, 2H), 2.61 (br. s, 1H), 2.26 (ddd, *J* = 8.0, 6.9, 2.7 Hz, 2H), 1.97–1.87 (m, 5H).

Synthesis of 1-hydroxyhept-6-yn-3-one (**C4**). To an acetone solution (42 mL) of **C3** (2.4 g, 14 mmol) was added *p*-TsOH (0.7 g, 3.5 mmol). The mixture was stirred at room temperature for 2 h before being extracted twice with EA. The resulting organic layers were washed with brine, filtered, dried over Na_2SO_4, and then concentrated. Following purification through flash column chromatography with silica gel using PE/EA (2:1, *V/V*), C4 was obtained as a colorless liquid with a yield of 80 % (0.4 g). TLC (PE/EA = 2:1, *V/V*): R_f = 0.36 [$KMnO_4$]. ^{1}H NMR (500 MHz, $CDCl_3$) δ 3.87 (t, *J* = 5.4 Hz, 2H), 2.74–2.68 (m, 5H), 2.46 (td, *J* = 7.2, 2.6 Hz, 2H), 1.96 (t, *J* = 2.7 Hz, 1H).

Synthesis of 2-(3-(but-3-yn-1-yl)-3*H*-diazirin-3-yl)ethan-1-ol (**C5**). To a flask containing **C4** (1.75 g, 14 mmol) was added NH_3 (7 M in MeOH; 30 mL, 210 mmol) at −40 °C. The mixture was stirred at −10 °C for 4 h in a sealed flask. Next, a solution of hydroxylamine-O-sulfonic acid (2.00 g, 18 mmol) in anhydrous MeOH (10 mL) was added dropwise over a period of 30 min with continuous stirring for 1 h at −10 °C. The mixture was left to reach room temperature overnight. To remove NH_3, N_2 was gently blown into the suspension. The resulting precipitates were filtered off and washed twice with methanol. The combined organic solutions were evaporated and dissolved in anhydrous MeOH (20 mL). Solution of NEt_3 (7 mL) and I_2 (7.5 g, 58 mmol, in 20 mL MeOH) was

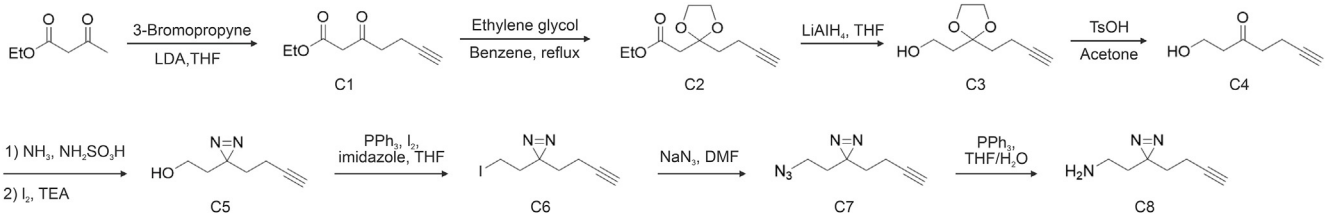

Scheme 1. The procedure of preparation of 2-(3-(but-3-yn-1-yl)-3H-diazirin-3-yl)ethan-1-amine (**C8**).

added by portion until the color of the reaction remained brown at 0 °C for 1 h. The EA-extracted mixture was subjected to a double extraction, and the resulting organic layers were combined and washed with brine, followed by drying over Na_2SO_4, filtration, and concentration. The resulting crude product was then purified using silica gel and PE/EA (4:1, *V/V*) to yield **C5** (676 mg, 35% yield) as a yellow oil. The spectral data are consistent with previous publication [28]. TLC (PE/EA = 2/1): R_f = 0.46 [UV | $KMnO_4$]. ^{1}H NMR (500 MHz, $CDCl_3$) δ 3.49 (t, J = 6.2 Hz, 2H), 2.04 (td, J = 7.4, 2.5 Hz, 2H), 2.00 (t, J = 2.6 Hz, 1H), 1.74–1.66 (m, 4H), 1.50 (br. s, 1H).

Synthesis of 3-(but-3-yn-1-yl)-3-(2-iodoethyl)-*3H*-diazirine (**C6**). I_2 (1.22 g, 4.8 mmol) was added to a solution of imidazole (819 mg, 12 mmol) and PPh_3 (1.16 g, 4.42 mmol) in CH_2Cl_2 (22 mL) at 0 °C. A solution of **C5** (552 mg, 4 mmol) in CH_2Cl_2 (5 mL) was added by dropwise. The reaction mixture was stirred for 4 h while being protected by aluminum foil. Afterward, the resulting solution was treated with aqueous $Na_2S_2O_3$ solution (25 mL) to quench the reaction, followed by extraction with EA twice. The combined organic layers were washed with brine, dried over Na_2SO_4, and concentrated. The residue was purified using silica gel chromatography with PE/EA (15:1, *V/V*) to afford the product **C6** as a colorless solid (840 mg, 85%). TLC (PE/EA = 10/1): R_f = 0.48 [$KMnO_4$]. ^{1}H NMR (500 MHz, $CDCl_3$) δ 2.87 (t, J = 7.6, 2H), 2.11 (t, J = 7.6, 2H), 1.99–2.04 (m, 3H), 1.67 (t, J = 7.2, 2H).

Synthesis of 3-(2-azidoethyl)-3-(but-3-yn-1-yl)-*3H*-diazirine (**C7**). NaN_3 (312 mg, 4.8 mmol) was added to a solution of **C6** (992 mg, 4 mmol) dissolved in N,N-dimethylformamide (DMF) (8 mL). The reaction was stirred at 70 °C for 5 h. After the reaction was fully completed, water was added to quench it, and then the mixture was subjected to EA extraction twice. The organic layers were combined, washed with brine, dried over Na_2SO_4, and concentrated. The residue was purified by silica gel using PE/EA (10/1) to afford **C7** as a colorless liquid (526 mg, 81% yield). ^{1}H NMR (500 MHz, $CDCl_3$) δ 3.22 (t, J = 6.1, 2H), 2.15–2.09 (m, 3H), 1.69–1.65 (m, 4H).

Synthesis of 2-(3-(but-3-yn-1-yl)-*3H*-diazirin-3-yl)ethan-1-amine (**C8**). To a THF/water solution (10:1 (*V/V*), 11 mL) of **C7** (488 mg, 3 mmol), PPh_3 (923 mg, 3,6 mmol) was added at room temperature. After being stirred for 24 h, the mixture was quenched with 1 M HCl (10 mL) once the reaction was completed, and then the resulting mixture was extracted with ether. After evaporating the volatiles, the residue was neutralized with 1 M NaOH and concentrated to yield **C8** (143 mg, 75% yield). The spectral data are in accordance with previous publication [27,28]. ^{1}H NMR (500 MHz, $CDCl_3$) δ 2.52 (td, J = 6.9, 1.0 Hz, 2H), 2.05–1.98 (m, 3H), 1.67–1.59 (m, 6H).

2.18. Synthesis of BA photoaffinity probe

BA (90 mg, 0.2 mmol) was dissolved in anhydrous DMF (10 mL), and then **C8** (33 mg, 0.24 mmol), 1-hydroxybenzotriazole (HOBT) (41 mg, 0.3 mmol), N-(3-dimethylaminopropyl)-N'-ethylcarbodiimide hydrochloride (EDCI) (58 mg, 0.3 mmol), and N,N-diisopropylethylamine (DIEA) (52 mg, 0.4 mmol) were added. The resulting solution was stirred for 9 h at 40 °C under nitrogen. Afterward, 20 mL of EA was added to the mixture, and the resulting organic layer was separated and washed successively with saturated $NaHCO_3$ and brine. The dried Na_2SO_4 was added, and the organic layer was then concentrated. The crude mixture was purified using semi-preparative high performance liquid chromatography (PR-HPLC) (60% MeCN with a flow rate of 8 mL/min) to yield BA probe (69 mg, 63 % yield) as a yellow solid. ^{1}H NMR (500 MHz, CD_3OD) δ 8.02–7.99 (m, 2H), 7.61–7.53 (m, 3H), 7.03 (s, 1H), 6.79 (s, 1H), 5.21 (d, J = 7.6 Hz, 1H), 4.06 (d, J = 9.3 Hz, 1H), 3.69–3.56 (m, 3H), 3.17 (t, J = 6.9 Hz, 2H), 2.17 (t, J = 2.7 Hz, 1H), 1.88 (td, J = 7.4, 2.7 Hz, 2H), 1.63 (q, J = 6.8 Hz, 2H), 1.54 (td, J = 7.5, 1.5 Hz, 2H); ^{13}C NMR (500 MHz, CD_3OD) δ 169.75, 164.86, 151.22, 150.02, 131.74, 131.16, 128.82, 126.18, 106.52, 104.31, 100.80, 94.42, 82.10, 75.53, 75.15, 72.77, 71.74, 68.88, 33.88, 31.85, 31.73, 26.49, 12.32; high resolution mass spectrometry (HRMS) (ESI) m/z calc. for $C_{28}H_{28}N_3O_{10}$ $[M + H]^+$ 566.1775, found 566.1770. Spectral copies are shown in Figs. S1–S3 Supplementary data (Multimedia component 1).

2.19. Pull-down and target validation with BA photoaffinity probe

Pull down experiment was carried out to identify the interaction between BA and β2-AR with some optimizations based on previous studies [30,31]. To simulate a stress state, MDA-MB-231 cells were incubated with Epi (10 μM) for 15 min and then lysed with M-PER lysis buffer containing protease and phosphatase inhibitors (Beyotime). The resulting supernatant (1–2 mg/mL protein) was divided into three parts and treated with either BA (100 μM) or DMSO at room temperature for 20–30 min. Each part was then incubated with either BA probe (100 μM) or DMSO (equal volume) at room temperature for another 20–30 min. In the competition group, lysates were treated with BA followed by BA probe treatment. The mixture was then subjected to ultraviolet (UV) radiation at 365 nm on ice for 15 min, followed by incubation with 100 μM biotin-azide, 2.5 mM sodium ascorbate, 1 mM $CuSO_4$, and 100 μM tert-butyl 2,2,2-trichloroacetimidate (TBTA) for 1 h at room temperature. Proteins were extracted using cold acetone overnight at −20 °C, washed with cold methanol and centrifuged at 18,000 *g* for 10 min at 4 °C twice. The resulting proteins were then dissolved in PBS supplemented with 0.4% sodium dodecyl sulfate (SDS) and incubated with streptavidin beads (Cat# 20357, Thermo Fisher) at room temperature for 2 h. The beads were washed with PBS containing 0.4% SDS, and the enriched proteins were denatured using 1 × loading buffer at 95 °C for 10 min and loaded onto 10% SDS-PAGE for Western blotting.

2.20. Prediction of BA binding sites on β2-AR

The docking analysis of BA and β2-AR was performed with AutoDockTools 1.5.6 software. The crystal structure of human β2-AR (Protein Data Bank code: 3NY8) was obtained from the Research Collaboratory for Structural Bioinformatics protein database. Discovery Studio 2019 software combined with the Chemistry at Harvard Macromolecular Mechanics force field were employed to predict the binding sites of BA on β2-AR. To identify the specific binding domain of β2-AR that interacts with BA, we used alanine-scanning mutagenesis based on the higher mutation energy in Discovery Studio 2019 software (Webster, TX, USA).

2.21. Behavior tests

Animal behaviors were assessed by investigators who were blinded to group allocation. To conduct the sucrose preference test, mice were granted access to both 1% sucrose solution and water concurrently. The preference for sucrose was computed by determining the proportion of the consumed sucrose solution in relation to the entire liquid intake. For the light-dark test, mice were placed in the dark box of a light-dark test device (Clever Sys Inc., Virginia, VA, USA). The light box was lit to a brightness of 400 lux. Each animal's duration spent in the light box, as well as entries made into both the light and dark boxes, was recorded for 5 min. An

animal entry to the box was defined as a mouse placing all four limbs onto the floor of either the dark or light box. The open field test was carried out in an open field apparatus with dimensions of 40 cm length × 40 cm width × 30 cm high, with a digital camera mounted directly above it. Mice were given time to adapt to the environment before being monitored. The small animal recording behavior analysis system I Topscanlite (Clever Sys Inc.) was set up the central and peripheral regions. Total distance traveled (mm), movement distance in the center (mm), time spent in the center (s), and frequency of crossing the center were monitored during a 5-min test session.

2.22. Ex vivo imaging system

To perform optical imaging, we used the IVIS Spectrum fluorescence imaging system (PerkinElmer, Waltham, MA, USA) to scan the excised lung tissues of mice. The system was equipped with filters for ex480/em520 visualization, and data acquisition and analysis were carried out using the manufacturer's Living Image 3.2© software.

2.23. Western blotting analysis

Western blotting assay was carried out according to our previous study [32]. The following primary antibodies were used in this study: N-cadherin (1:500, Cat # sc-59987, Santa Cruz, Dallas, TX, USA), E-cadherin (1:500, Cat # AF0131, Affinity, Shanghai, China), Vimentin (1:500, Cat # sc-6260, Santa Cruz), p-FAK (1:500, Cat # AF3398, Affinity), p-SRC (1:500, Cat # sc-81521, Santa Cruz), RhoA (1:500, Cat # sc-418, Santa Cruz), FAK (1:500, Cat # sc-1688, Santa Cruz), SRC (1:500, Cat # sc-8056, Santa Cruz), β2-AR (1:500, Cat # AF6117, Affinity; 1:1000, ab61778, Abcam, Cambridge, MA, USA), and glyceraldehyde-3-phosphate dehydrogenase (GAPDH) (1:500, Cat # 10494-1-AP, Proteintech, Wuhan, China).

2.24. Hematoxylin-eosin (HE) staining

Tissue specimens were prepared for analysis by sectioning at 4 μm thickness and deparaffinizing in xylene followed by rehydration in a gradient ethanol solution and tap water. After being sectioned, the samples were subjected to hematoxylin reagent staining for 3 min, then briefly destained in 1% hydrochloric acid-alcohol solution for 3 s, and finally rinsed using running tap water. Next, the samples were counterstained with eosin for 5 min and dehydrated before being mounted for observation. Finally, image acquisition was performed using Mantra quantitative pathology workstation (PerkinElmer).

2.25. Immunohistochemistry (IHC)

Paraffin-embedded tissue specimens were cut into 5 μm thickness and subjected to deparaffinization with xylene, rehydration, and antigen retrieval in sodium citrate. To block endogenous peroxidase, the sections were treated accordingly. Primary antibodies against Ki67, E-cadherin, N-cadherin, p-FAK, p-SRC, or RhoA (1:50 dilution) were added and incubated overnight at 4 °C, followed by the appropriate secondary antibody. The sections were subjected to staining using a DAB kit (ZSGB-BIO, Beijing, China) until the desired level of stain intensity was attained. After counterstaining with hematoxylin, the sections were dehydrated, and mounted. Image acquisition was performed using Mantra Quantitative Pathology workstation (PerkinElmer), and Image J software was used to analyze protein expression levels.

2.26. Immunofluorescence (IF) assay

IF assay was carried out according to our previous study [32]. The following primary antibodies were used in this study: E-cadherin (1:100, Cat # AF0131, Affinity), N-cadherin (1:100, Cat # sc-59987, Santa Cruz), matrix metalloproteinase 2 (MMP2) (1:1000, Cat # 3853, Cell Signaling Technology, Danvers, MA, USA), p-FAK (1:1000, Cat # 9330, Cell Signaling Technology), or p-PXN (1:1000, Cat # 2451, Cell Signaling Technology). And the corresponding secondary antibodies were used: goat anti-rabbit IgG H&L (Alexa Fluor® 488) (1:1000, ab150077, Abcam) or goat anti-mouse IgG H&L (FITC) (1:1000, ab6785, Abcam). Finally, the cells were visualized by a fluorescence microscope (Zeiss, Jena, Germany).

2.27. Concentration detection of BA in tumors

4T1 cells were inoculated to establish an *in situ* mouse model of breast cancer. When tumors reached 100 cm^3, BA was administered by intragastric administration at 100 mg/kg. Then the mice were sacrificed at 10 min, 30 min, 1 h, 4 h, 7 h, and 10 h, and the tumors were harvested. The tumors were subjected to LC-MS/MS (AB SCIEX, Framingham, MA, USA) to detect the concentration of BA in tumors at different time points.

2.28. Statistical analysis

GraphPad Prism 8.0 (La Jolla, CA, USA) was utilized for statistical analysis. Pairwise comparison was conducted using two-tailed unpaired *t*-tests, while one-way analysis of variance (ANOVA) was utilized for comparisons among multiple groups. Statistical significance was set at $P < 0.05$. The results were presented as mean ± standard deviation (SD).

3. Results

3.1. BA suppressed stress hormone Epi-mediated breast cancer cell migration and invasion in vitro

To evaluate the role of BA in chronic stress-induced breast cancer metastasis, we initially constructed *in vitro* stress hormones-induced breast cancer metastasis model. Since psychosocial stress-induced cancer progression was mainly mediated by the excess activation of the SNS releasing Epi and NE and to a lesser degree by the HPA axis releasing stress hormones [5,6], the levels of NE, Epi, and corticosterone (the primary glucocorticoid stress hormone in rodents that is equivalent to Cort in humans [33]) in serum were firstly measured. Their contents were indeed increased in CRS- and CUMS-induced breast cancer metastatic mice model (Figs. 1A and B). The ability of these neurotransmitters and stress hormone on the metastatic progression of breast cancer cell displayed that Epi had the most deleterious results (Fig. S1). We used Epi-induced metastasis model of breast cancer cell to measure the inhibitory effect of BA. Notably, BA not only suppressed the migration ability of breast cancer cells on plane wound healing and transwell migration assays (Figs. 1C–F), but also significantly suppressed the invasion ability on a 3D spheroid assay in a concentration-dependent manner (Figs. 1G and H).

3.2. BA directly targets β2-AR

To investigate the underlying mechanisms of BA contributing to the inhibition of cell migration ability, we performed DARTS assay [23,34] by using the lysate of MDA-MB-231 cells pre-treated with Epi (Fig. S2). Further combined analysis with the genes related to breast cancer metastasis and Epi via mining of GeneCards and

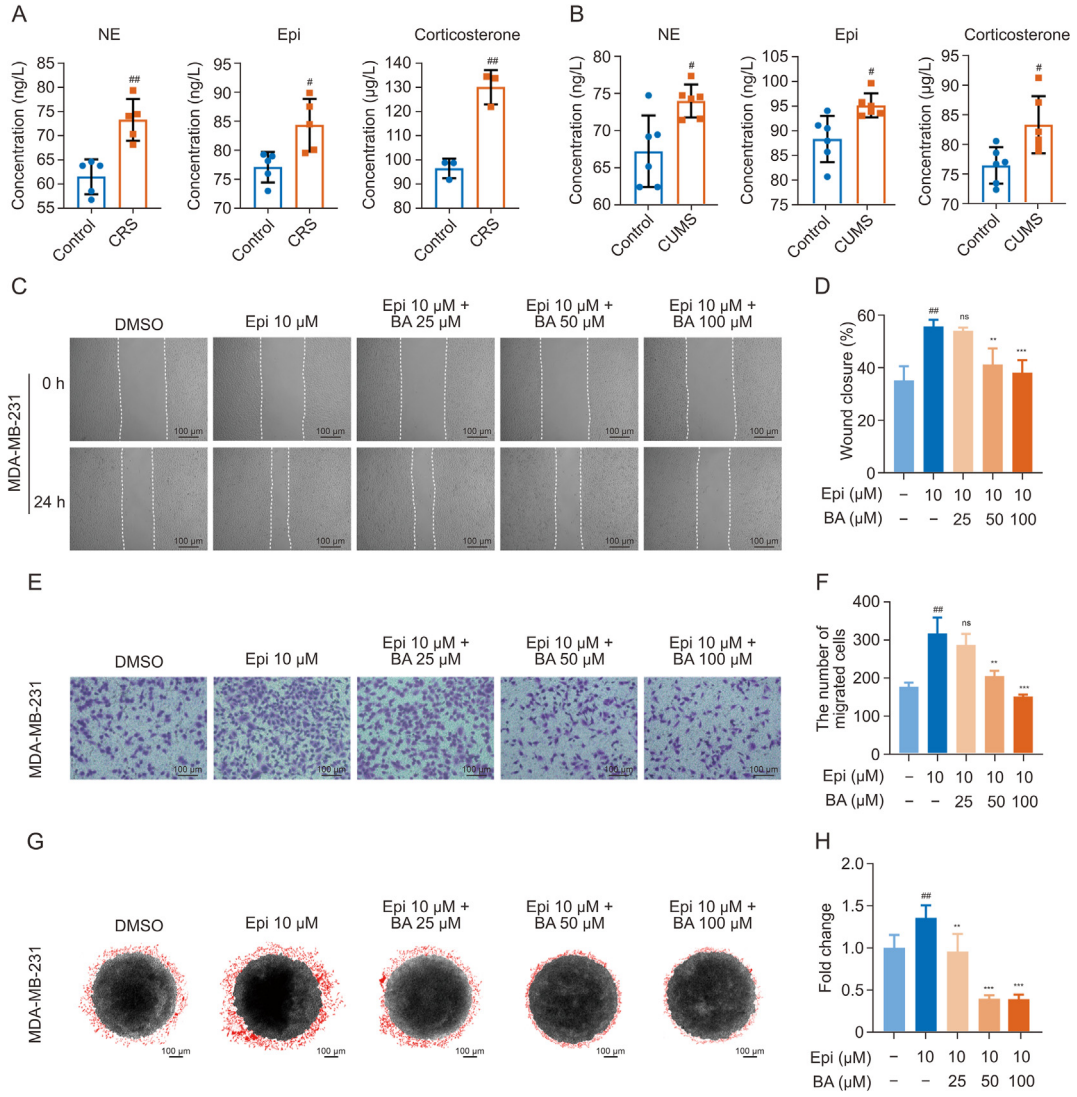

Fig. 1. Baicalin (BA) can suppress stress hormone epinephrine (Epi)-promoted migration and invasion of breast cancer cells *in vitro*. (A, B) The levels of stress hormones norepinephrine (NE), Epi, and corticosterone in serum were detected in chronic restraint stress (CRS) (A) ($n = 5$) and chronic unpredictable mild stress (CUMS) (B) ($n = 6$) induced breast cancer metastatic mice model. (C, D) Wound healing assay was performed to evaluate the effects of BA on stress hormone Epi-induced migration ability of MDA-MB-231 cells (C), which were quantified in (D). (E, F) Transwell migration analysis was conducted to determine the effects of BA on Epi-enhanced migration ability of MDA-MB-231 cells (E), which were quantified in (F). (G, H) A 3D tumor spheroid invasion assay was constructed to detect the effects of BA on Epi-promoted invasive ability of MDA-MB-231 cells (G), which were quantified in (H). $^{\#}P < 0.05$, $^{\#\#}P < 0.01$ vs. control or DMSO; $^{**}P < 0.01$, $^{***}P < 0.001$ vs. Epi; ns: no significance, $n = 3$. DMSO: dimethyl sulfoxide.

OMIM database, six overlapping proteins (low molecular weight phosphotyrosine protein phosphatase (LMW-PTP), β2-AR, RAC-alpha serine/threonine-protein kinase (PKB), DNA-(apurinic or apyrimidinic site) endonuclease (APEN), cytochrome c (CYCS), and mitogen-activated protein kinase 1 (MAPK1)) were identified (Fig. 2A, and Tables S1–S3). Then the minimum binding energy with BA was further determined by AutoDockTools. It was found that β2-AR exhibited the lowest binding energy (−7.37) (Fig. 2B), which hints that β2-AR was the strongest candidate target of BA within BA-mediated suppressive effects on stress hormone-promoted migration of breast cancer cell. To evaluate the direct binding of BA to β2-AR, we synthesized BA photoaffinity probe (Fig. 2C) and determined its effects on breast cancer cell viability and migration. As shown in Figs. S3A–C, BA photoaffinity probe had little effect on breast cancer cell viability and displayed similar effects on Epi-promoted migration of breast cancer cell with BA. And pull-down experiments indicated that β2-AR was pulled down by BA probe (Fig. 2D). Gradient concentrations of pronase were used to verify the proteolytic inhibition of BA (Figs. 2E and F).

To further verify BA directly binds to β2-AR and inhibits its activity, CETSA results showed that BA treatment efficiently protected β2-AR from temperature-dependent degradation (Figs. 2G and H), whereas the MST assay calculated the K_d value of BA to β2-AR was 6.9 μM (Fig. 2I). BLI also confirmed BA directly bound to β2-AR (Fig. 2J).

3.3. BA binds to the Phe-193 and Phe-289 of β2-AR

Molecular docking results showed that BA can bind with β2-AR (Fig. S4), and that several amino acid sites in the binding pocket of ICI118551 with β2-AR, including Tyr-316, Asn-312, Asp-113, Phe-289, Phe-193 and Tyr-308 might be the binding sites of BA (Fig. 3A). Based on the virtual dynamic simulation, Phe-289, Asn-312, and Phe-193 mutated into alanine were indicative to have

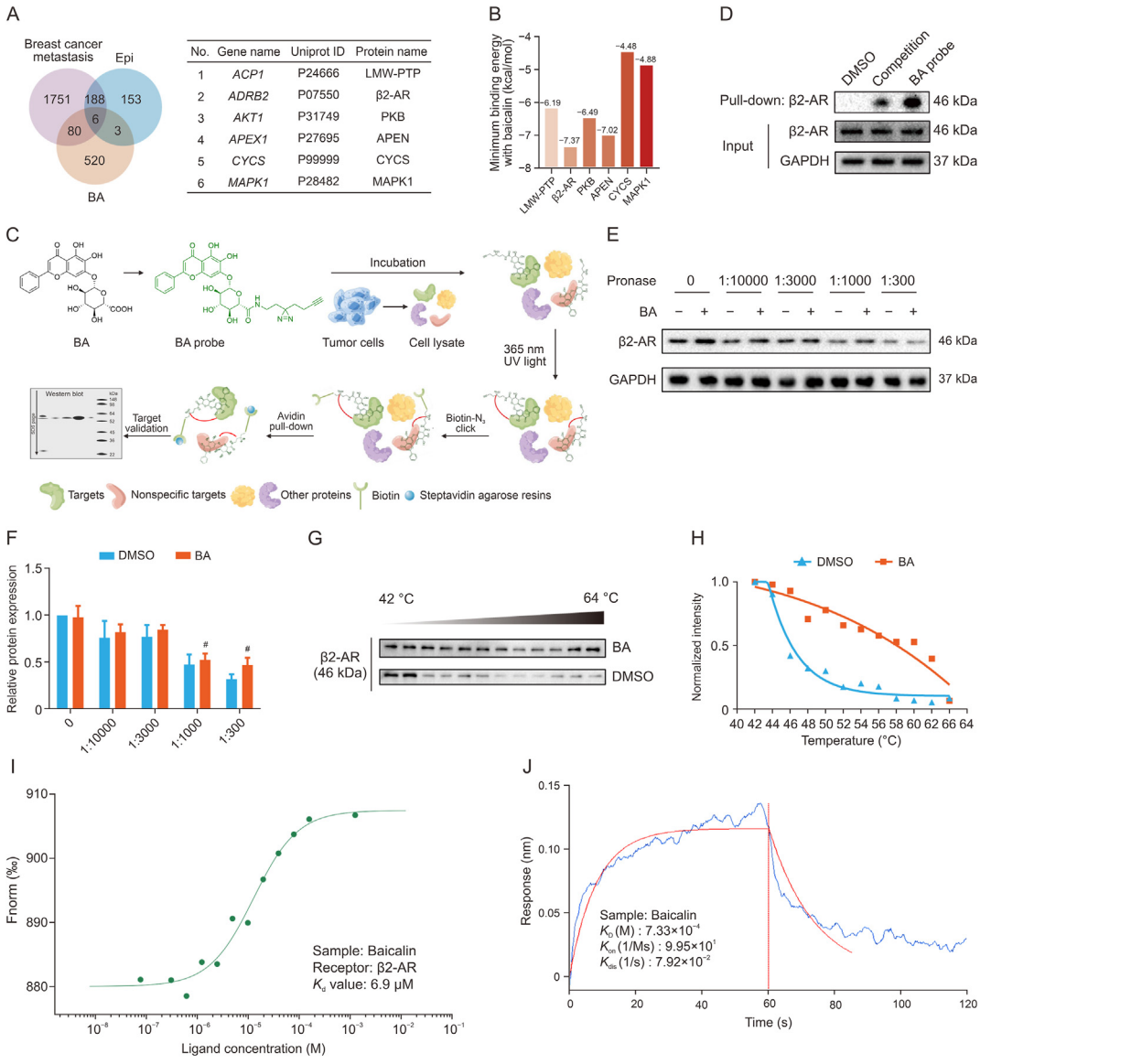

Fig. 2. Baicalin (BA) could target β2-adrenergic receptor (β2-AR). (A) The Venn diagram showed the targets of BA, epinephrine (Epi), and breast cancer metastasis, highlighting six of the overlapping targets (LMW-PTP: Low molecular weight phosphotyrosine protein phosphatase; PKB: RAC-alpha serine/threonine-protein kinase; APEN: DNA-(apurinic or apyrimidinic site) endonuclease; CYCS: Cytochrome c; MAPK1: Mitogen-activated protein kinase 1). (B) The binding energy of BA to the six potential target proteins in (A) using AutoDockTools. (C) Structure of BA photoaffinity probe and the course of pull-down experiment using BA photoaffinity probe. (D) Pull-down experiments were performed to detect the interaction between BA photoaffinity probe and β2-AR protein. Competition group: BA and BA probe. (E–J) drug affinity responsive target stability (DARTS) (E, F), cellular thermal shift assay (CETSA) (G, H), micro scale thermophoresis (MST) (I), and bio-layer interferometry (BLI) (J) were conducted to evaluate the direct binding of BA to β2-AR. $^{\#}P < 0.05$ vs. DMSO, $n = 3$. GAPDH: glyceraldehyde-3-phosphate dehydrogenase; DMSO: dimethyl sulfoxide.

high mutation energy (Fig. 3B). Considering the π-π stacking between flavonoid scaffold and phenyl moieties, we speculated that Phe-193 and Phe-289 are the binding sites of BA and responsible for BA-mediated effects on stress hormone-induced breast cancer cell migration. First, simultaneous mutations of F193A and F289A exhibited the highest mutation energy (2.61 kcal/mol) in various combination of above key residues (Fig. 3C). Next, DARTS and CETSA assays illustrated that BA did not bind to the β2-AR with both Phe-289 and Phe-193 mutated to alanine (Figs. 3D–G). Finally, transfection of β2-AR with Phe-289 and Phe-193 mutation plasmid to the MDA-MB-231 ADRB2^{KO} cells not only greatly diminished the BA-caused inhibition of the cell migration and invasion induced by Epi treatment (Figs. 3H–M), but also weakened the suppression of cAMP level by BA treatment in the cell model with wild type of β2-AR (Fig. 3N). Taken together, these results validated that Phe-193 and Phe-289 are the key residues in the binding domain.

3.4. BA restrained β2-AR activation and breast cancer cell migration mediated by β2-AR activation in vitro

We further explore whether BA could induce β2-AR inactivation. Expectedly, upregulation of cAMP upon activation of β2-AR using nonselective β2-AR agonist ISO or the specific β2-AR agonist SAL was reversed by the treatment of BA in MDA-MB-231 and 4T1 cells, respectively (Figs. 4A and B), while BA alone had no effect on the intrinsic activity of β2-AR (Fig. 4A) and the protein level of β2-AR had no change in these assays (Figs. 4C–F).

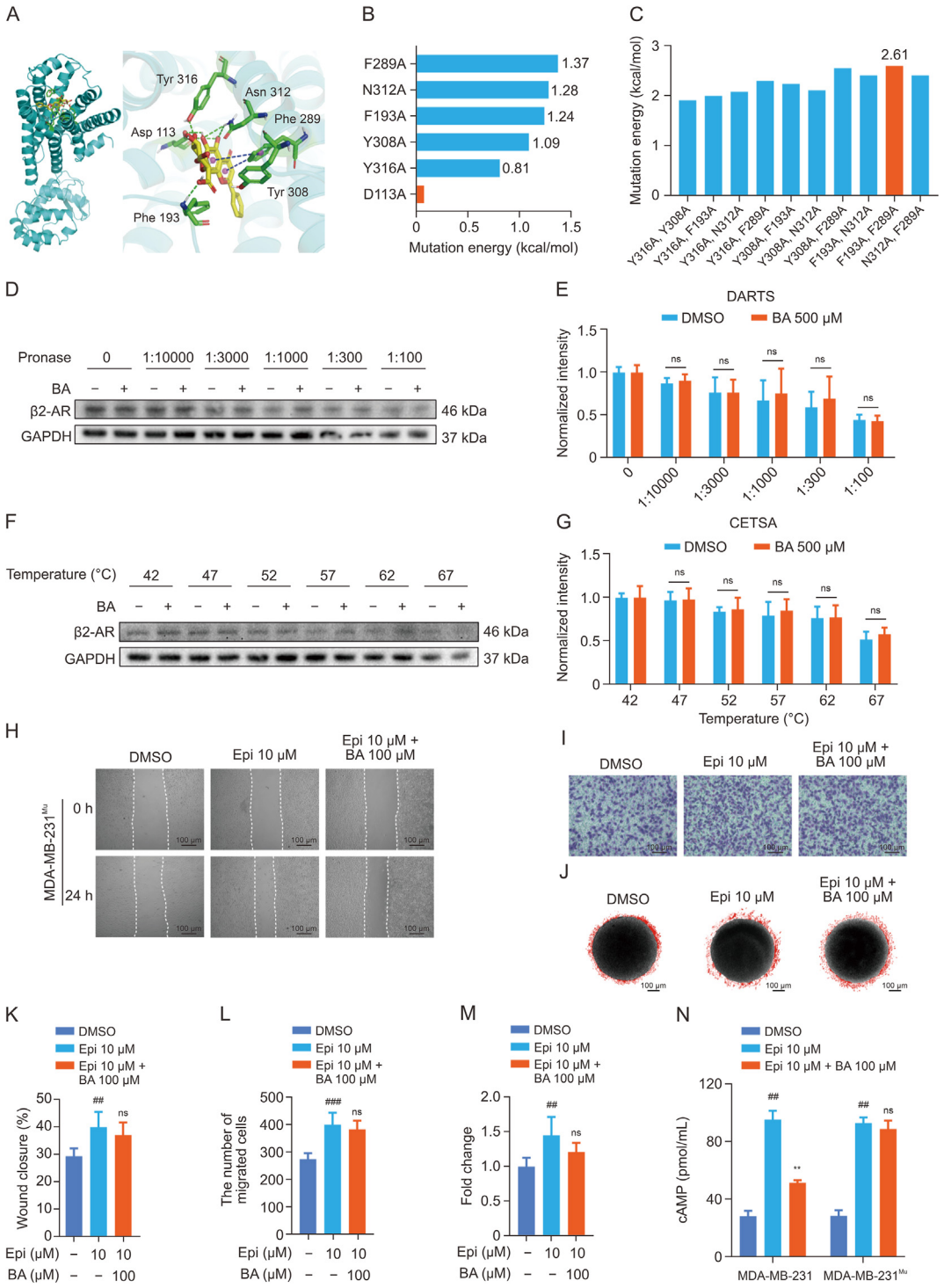

Fig. 3. Baicalin (BA) binds to Phe-193 and Phe-289 sites of β2-adrenergic receptor (β2-AR). (A) The binding pockets and the interacting amino acids of BA with β2-AR by molecular docking. (B, C) The mutation energy of β2-AR was calculated for β2-AR with single amino acid mutation (B) and double mutations (C) using virtual mutations. (D–G) Drug affinity responsive target stability (DARTS) (D, E) and cellular thermal shift assay (CETSA) (F, G) assays were performed to evaluate the binding of BA to β2-AR with F289A and F193A mutations. (H–M) β2-AR-null MDA-MB-231 cells overexpressing β2-AR with F289A and F193A mutations were treated with epinephrine (Epi) plus BA or not, and subjected to wound healing (H), transwell migration (I), and 3D tumor spheroid invasion (J) assays, which were quantified in (K), (L), and (M), respectively. (N) Cyclic adenosine monophosphate (cAMP) level was examined in MDA-MB-231 and MDA-MB-231^{Mu} cells treated with Epi plus BA or not. $^{\#\#}P < 0.01$, $^{\#\#\#}P < 0.001$ vs DMSO; $^{**}P < 0.01$ vs. Epi; ns: no significance.

Furthermore, Epi elicited a sigmoidal dose-response of cAMP level with a pEC_{50} of −7.5. In the presence of BA, the Epi pEC_{50} increased to −6.4, and the maximal cAMP efficacy (*Emax*) reduced (Fig. 4G). In agreement with this, cAMP level increased with BA plus the gradual increase of SAL, but it could not reach the maximum level of using SAL alone (Fig. 4H), suggesting BA inhibits β2-AR function in a noncompetitive manner.

Next, we explore whether BA halted β2-AR activation-induced breast cancer cell migration. It has been reported that β2-AR activation could promote breast cancer metastasis, and therefore we

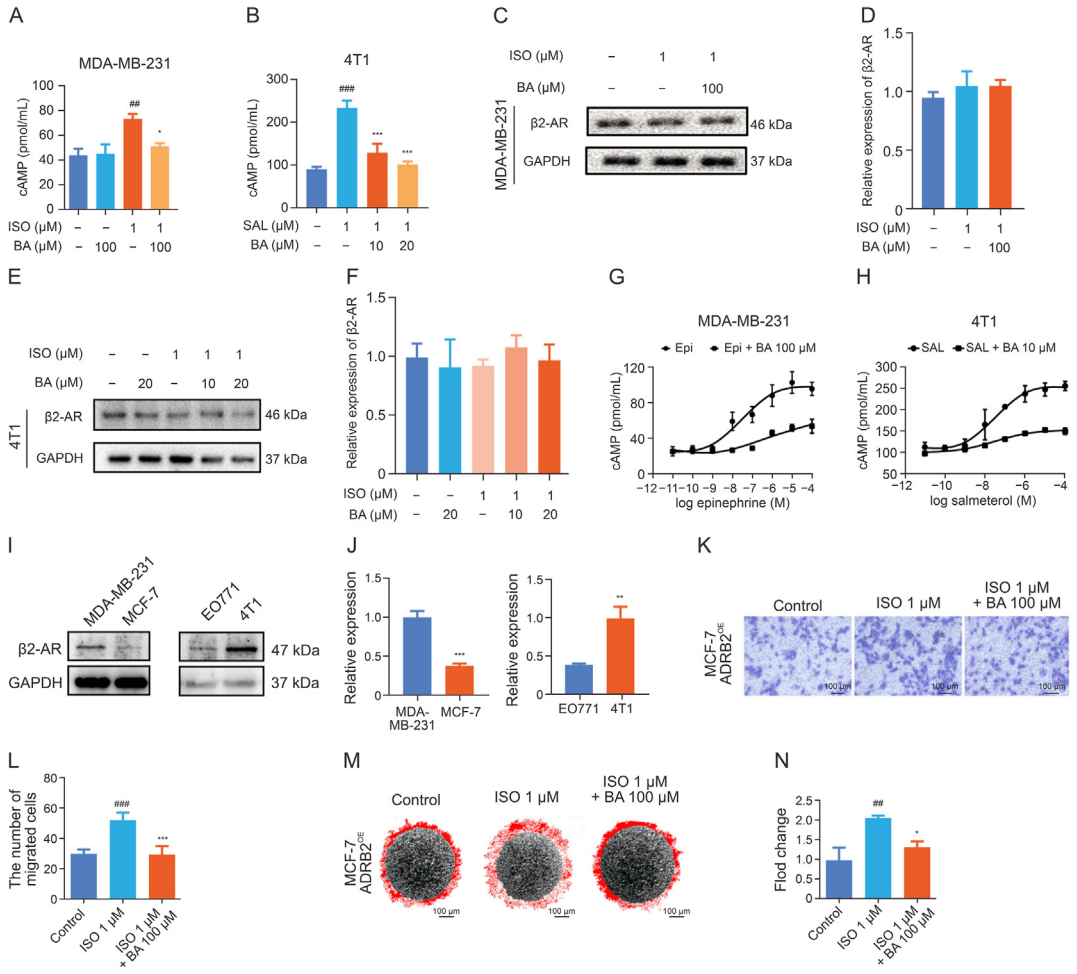

Fig. 4. Baicalin (BA) prohibits β2-adrenergic receptor (β2-AR) activation and breast cancer cell migration mediated by β2-AR activation *in vitro*. (A, B) Cyclic adenosine monophosphate (cAMP) level was measured in MDA-MB-231 (A) and 4T1 (B) cells incubated with BA, isoprenaline (ISO)/salmeterol (SAL), or BA plus ISO/SAL, respectively. $^{\#\#}P < 0.01$, $^{\#\#\#}P < 0.001$ vs. control; $^{*}P < 0.05$, $^{***}P < 0.001$ vs. ISO or SAL, $n = 3$. (C, D) β2-AR protein expression was detected in MDA-MB-231 cells treated with ISO as well as BA or not (C), and quantified (D). (E, F) β2-AR protein expression was detected in 4T1 cells treated with ISO, BA, or BA plus ISO (E), and quantified (F). (G) cAMP level was examined in MDA-MB-231 cells incubated with epinephrine (Epi), or BA plus the increasing concentration gradients of Epi. (H) cAMP level was determined in 4T1 cells treated with SAL, and BA plus the increasing concentration gradients of SAL. (I, J) β2-AR protein expression was detected in different types of cells. $^{***}P < 0.001$ vs. MDA-MB-231; $^{**}P < 0.01$ vs. EO771, $n = 3$. (K , L) MCF-7 cells with β2-AR overexpression were subjected to detection of migration ability upon treated with ISO as well as BA or not (K), and quantified (L). (M, N) A 3D-tumor spheroid invasion assay was constructed to detect invasive ability of MCF-7 cells with β2-AR overexpression (M), which was quantified in (N). $^{\#\#}P < 0.01$, $^{\#\#\#}P < 0.001$ vs. control; $^{*}P < 0.05$, $^{***}P < 0.001$ vs. ISO, $n = 3$.

initially analyzed β2-AR expression in different cell types. It is strikingly to find that β2-AR was lowly expressed in MCF-7 and EO771 cells, which responsively showed feeble metastatic ability. In contrast, we detected that relative high level of β2-AR expression agreed to high potential of metastasis, such as MDA-MB-231 and 4T1 cells (Figs. 4I and J). Thus, we knocked ADRB2 out from MDA-MB-231 cells and overexpressed ADRB2 in MCF-7 cells, respectively (Fig. S5A). As expected, ectopic expression of β2-AR increased the migration and invasive ability of MCF-7 cells, while knockout of β2-AR resulted in the opposite effect in MDA-MB-231 cells (Figs. S5B–E).

These above engineered cell lines were used to study whether BA suppressed β2-AR activation-mediated breast cancer cell metastasis. We found that BA significantly suppressed β2-AR activation-induced migration in MDA-MB-231 cells, while did not affect the ability of cell migration and invasion in the absence of β2-AR agonist ISO (Figs. S5F–I). Notably, such effect did not appear in MCF-7 cells with almost no β2-AR expression (Figs. S5F–I). We further evaluated these effects in MCF-7 cells with β2-AR overexpression and found that overexpression of β2-AR resensitized cells to the treatment of β2-AR agonist, while ISO-induced the migration and invasion ability was reversed by BA treatment (Figs. 4I and J). Briefly, these results confirmed that BA halted β2-AR activation and thus inhibited β2-AR activation-induced breast cancer cell migration and invasion *in vitro*.

3.5. BA hampering EMT in β2-AR activation-induced breast cancer cell migration

Interestingly, we found that the morphology of MDA-MB-231 cells changed from long spindle shape into spherical shape upon β2-AR knockout, and the activation of β2-AR transformed the cell morphology of 4T1 cells from tight junction into pseudopodia and long spindle shape (Fig. 5A). Additionally, linked omics database (www.linkedomics.org/login.php) showed that most genes related to β2-AR can be enriched in the function of extracellular matrix structure (Figs. 5B, and S6A–C), which was verified by the expression of matrix metalloproteinase (MMP) family members

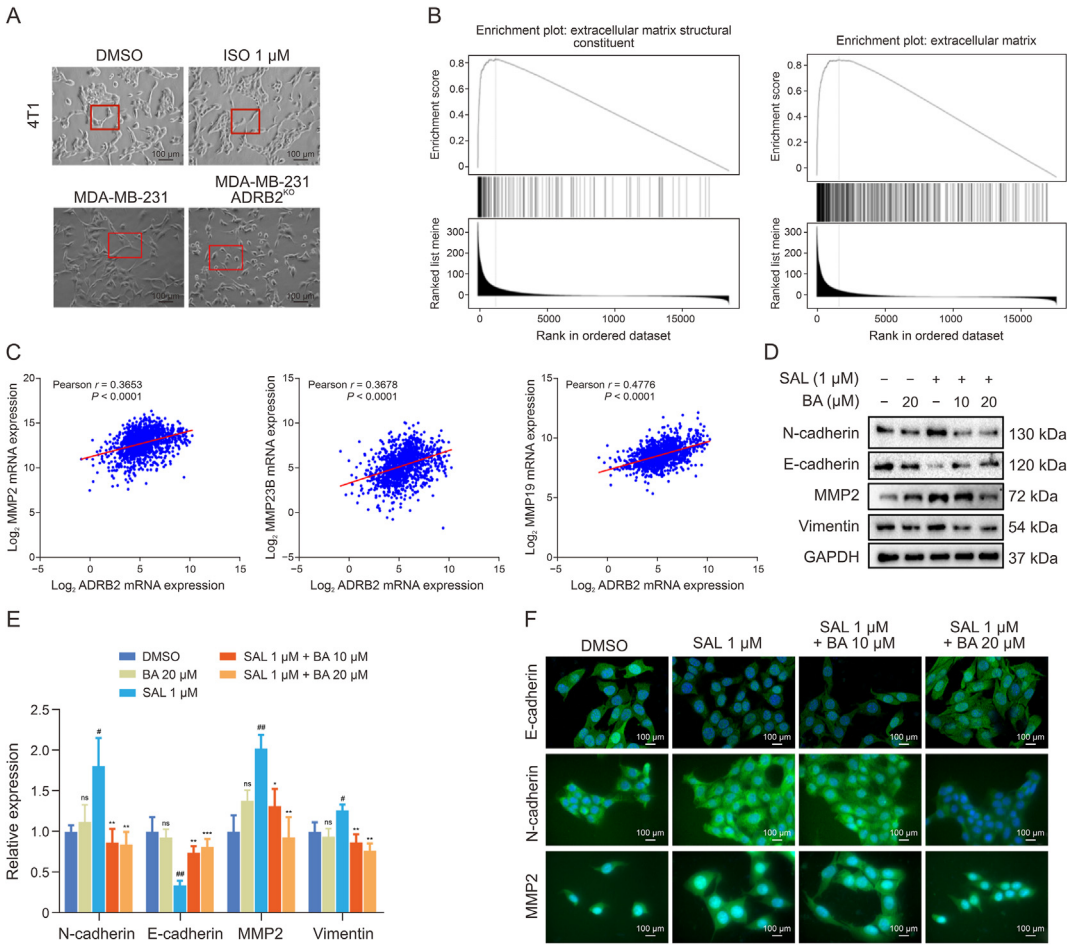

Fig. 5. Baicalin (BA) impeded β2-adrenergic receptor (β2-AR) activation-induced breast cancer cell migration via hampering epithelial-mesenchymal transition (EMT). (A) Representative images of 4T1 cells with or without isoprenaline (ISO) treatment, and MDA-MB-231 cells with or without β2-AR knockout. (B) Linked omics database was used to analyze the most related genes to β2-AR. (C) The correlation between β2-AR and matrix metalloproteinase (MMP) family members expression was analyzed using The Cancer Genome Atlas (TCGA) datasets. (D, E) The protein expression levels of EMT markers (E-cadherin, N-cadherin, MMP2, and Vimentin) were detected in 4T1 cells treated with BA, salmeterol (SAL), or SAL plus BA (D), and quantified (E). $^{\#}P < 0.05$, $^{\#\#}P < 0.01$ vs. DMSO; $^{*}P < 0.05$, $^{**}P < 0.01$, $^{***}P < 0.001$ vs. SAL; ns: no significance, $n = 3$. (F) Immunofluorescence (IF) assay was carried out to detect EMT markers' expression in the cells described in (D).

using The Cancer Genome Atlas (TCGA) datasets (Fig. 5C). These results prompted us to consider whether EMT process was engaged in BA-mediated suppression on β2-AR activation-induced breast cancer cell migration. As expected, upregulation of EMT markers, N-cadherin, MMP2 and Vimentin, and downregulation of E-cadherin induced by β2-AR agonist were abrogated by BA treatment (Figs. 5D and E). IF assay obtained a consistent result (Fig. 5F).

3.6. BA reduced chronic stress-induced breast cancer metastasis *in vivo*

To assess whether the inhibitory effects of BA on stress hormone-induced breast cancer cell migration existed *in vivo*, we generated depression models by applying CUMS and CRS, both of which have been widely used as animal models of depression. The establishments of these two depression models were evidenced by the decrease of sucrose preference, reduced time in the light box in light-dark box test, and shorter central time spent in the open field test as well as reduced concentration of DA and 5-HT in hippocampus (Fig. S7). LC-MS/MS was employed to test the concentration of BA in tumors and showed that the peak concentration of BA in tumor was 276 ng/g 1 h after BA treatment (Fig. S8). Mouse breast cancer cell line 4T1 with GFP tracker were inoculated to the CUMS mice to monitor the metastasis of breast cancer cells (Fig. 6A). By using *ex vivo* imaging system, we found that BA (50 and 100 mg/kg) significantly suppressed CMUS-induced orthotopic metastasis of 4T1 cells to the lung tissue (Figs. 6B and C). HE staining and IHC experiment obtained a consistent result, which was evidenced by the decreased number of lung metastatic nodes and Ki67-positive cell ratio (Figs. 6D–F). Similar results were obtained in the human breast cancer cell line MDA-MB-231 orthotopic breast tumor combined with CRS model (Fig. 7). Furthermore, breast cancer metastatic model using tail vein injection displayed a consistent result, as evident by the fact that BA significantly retarded CRS-promoted metastasis of MDA-MB-231 cells to the lung and liver using HE and IHC for Ki-67 staining assays (Figs. S9A–G). Besides, *ex vivo* imaging system, HE and IHC for Ki-67 staining indicated that BA attenuated CUMS-induced metastasis of EO771 cells to the lung (Figs. S9H–M). Moreover, we verified that BA alone did not alter orthotopic breast cancer metastasis of MDA-MB-231 cells (Fig. S10). In brief, these results implied that BA reduced chronic stress-induced breast cancer metastasis *in vivo*.

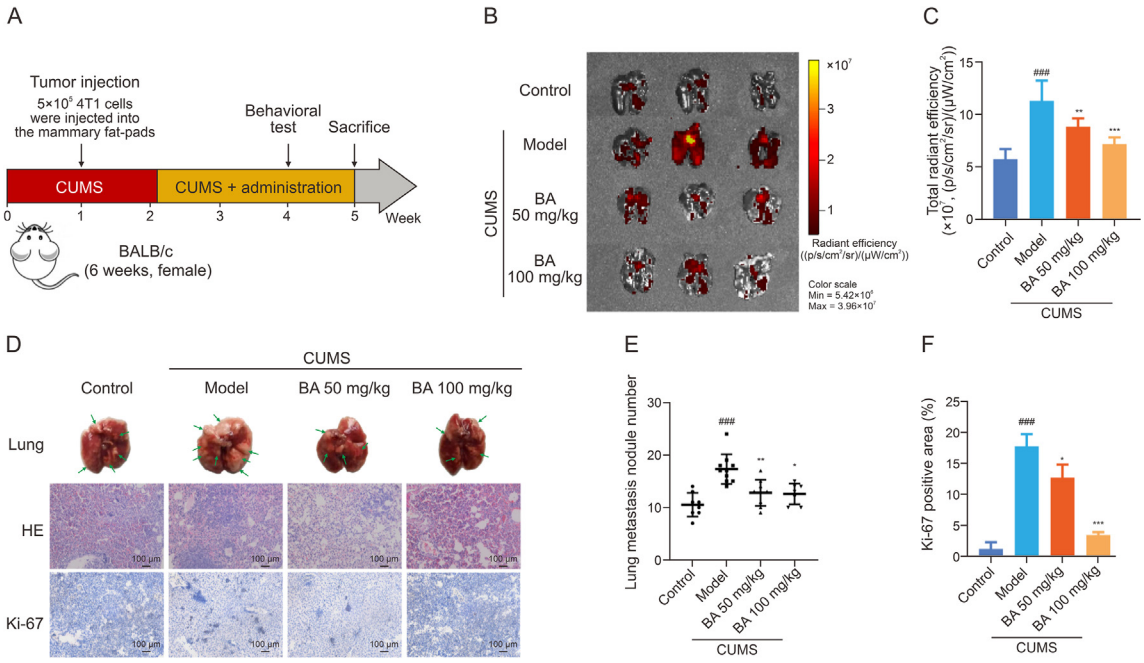

Fig. 6. Baicalin (BA) reduced chronic unpredictable mild stress (CUMS)-induced metastasis *in situ* tumor model constructed by mouse breast cancer cell line 4T1. (A) Time course of CUMS, tumor implantation and administration of BA. (B) Illustrative examples of *ex vivo* imaging of metastatic sites in lung tissues. (C) Statistics of total radiant efficiency in (B). (D) Representative images of lung, and hematoxylin-eosin (HE) and immunohistochemistry (IHC) for Ki-67 staining in lung. Black arrow: obvious metastases. (E) Metastatic nodes in lung tissues were quantified. (F) Ki67 positive cells were quantified in lung tissues. $^{###}P < 0.01$ vs. control; $^{*}P < 0.05$, $^{**}P < 0.01$, $^{***}P < 0.001$ vs. model. Control group, $n = 8$, CUMS group, $n = 10$, BA 50 mg/kg group, $n = 8$, BA 100 mg/kg group, $n = 7$.

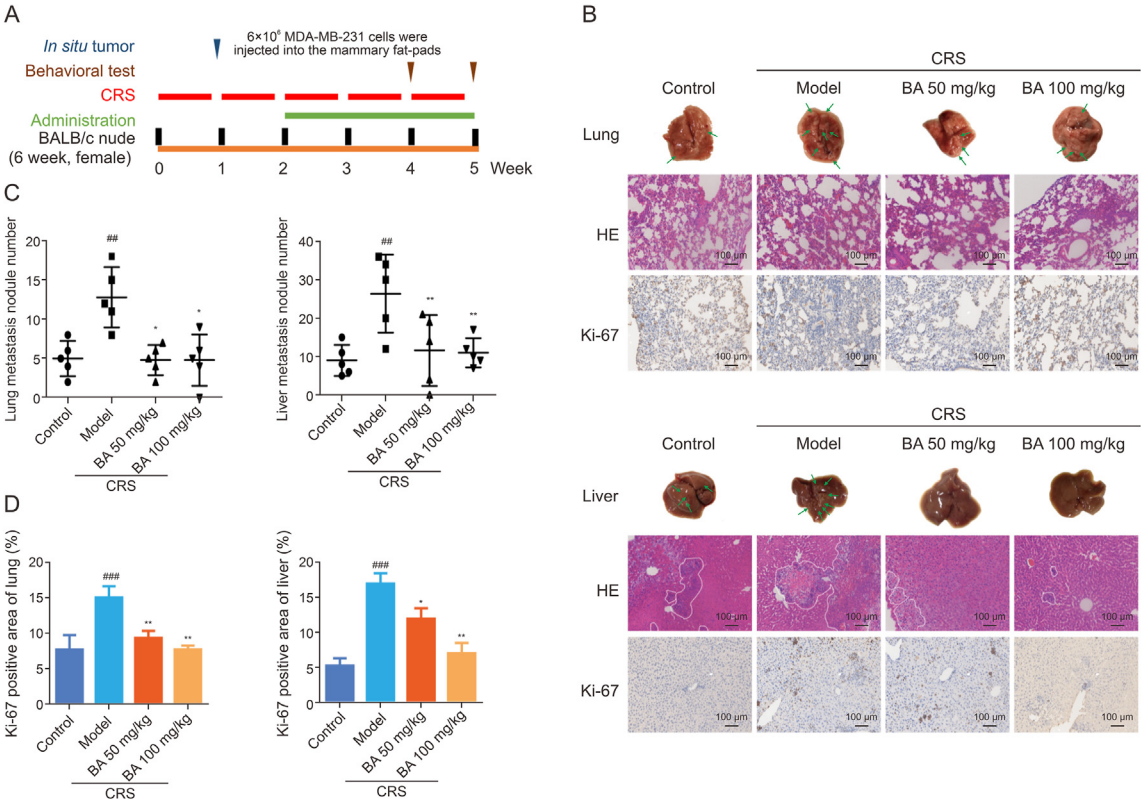

Fig. 7. Baicalin (BA) reduced chronic restraint stress (CRS)-induced metastasis *in situ* tumor model derived from human breast cancer cell line MDA-MB-231. (A) Time course of the effects of BA on breast cancer metastasis *in situ* CRS tumor model. (B) Representative images of lung, and liver, and hematoxylin-eosin (HE) and immunohistochemistry (IHC) staining for Ki-67 in lung (upper) and liver (lower). Black arrow: obvious metastases. (C) Metastatic nodes in lung and liver tissues were quantified. (D) Ki-67 positive cells were quantified in lung and liver tissues. $^{##}P < 0.01$, $^{###}P < 0.001$ vs. control; $^{*}P < 0.05$, $^{**}P < 0.01$ vs. model. $n = 5$.

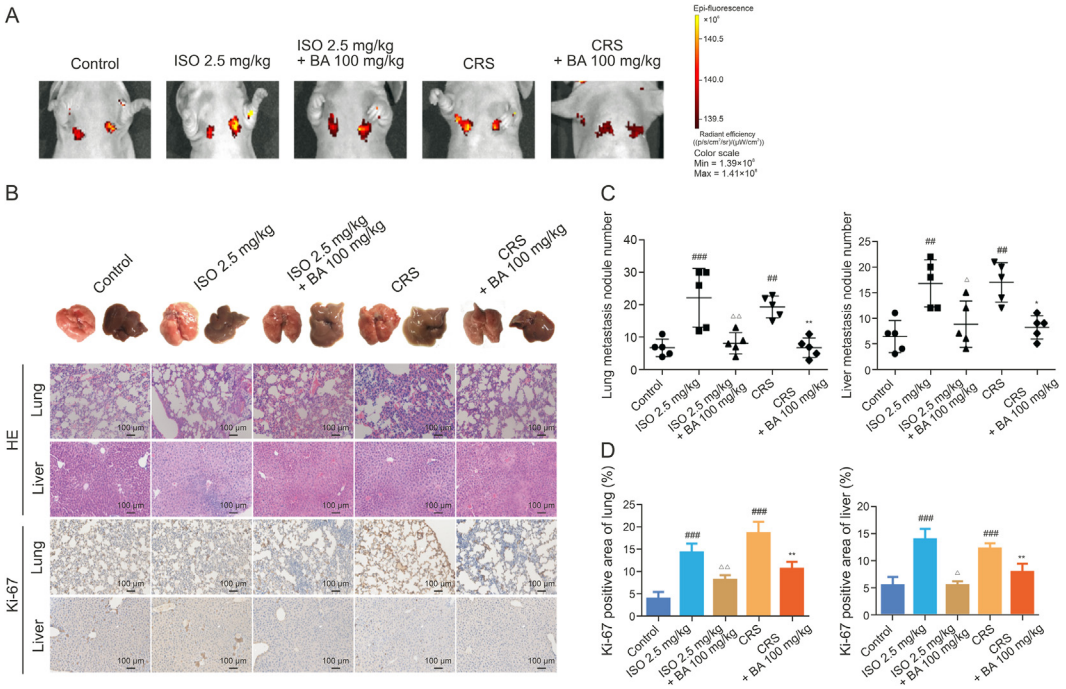

Fig. 8. Baicalin (BA) attenuates chronic stress-induced breast cancer metastasis by suppressing β2-adrenergic receptor (β2-AR) activation *in vivo*. (A) Illustrative examples of *ex vivo* imaging of metastatic sites in lung tissues in intravenous metastatic model derived from MCF-7 cells with β2-AR and green fluorescent protein (GFP) overexpression treated with isoprenaline (ISO) alone or plus BA, or with chronic restraint stress (CRS) alone or combined with BA. (B) Representative images of lung, and liver, and hematoxylin-eosin (HE) and immunohistochemistry (IHC) staining for Ki-67 in lung and liver. (C) Metastatic nodes in lung and liver tissues were quantified. (D) Ki-67 positive cells were quantified in lung and liver tissues. $^{\#\#}P < 0.01$, $^{\#\#\#}P < 0.001$ vs. control; $^{\triangle}P < 0.05$, $^{\triangle\triangle}P < 0.01$ vs. ISO; $^{*}P < 0.05$, $^{**}P < 0.01$ vs. CRS. $n = 5$.

3.7. BA impeded chronic stress-induced breast cancer metastasis via suppressing β2-AR activation in vivo

To evaluate whether BA hampered chronic stress-induced breast cancer metastasis *in vivo* also via inhibiting β2-AR activation, MCF-7 cells (almost no β2-AR expression) and β2-AR-overexpressed MCF-7 cells were inoculated to establish an *in situ* mouse model of breast cancer metastasis. Using *ex vivo* imaging system, it was found that BA significantly suppressed ISO- or chronic stress-induced orthotopic breast cancer metastasis on the β2-AR-overexpressed MCF-7 mice (Fig. 8A). HE staining and IHC experiments obtained a consistent result, which was evidenced by the decreased number of metastatic nodes and Ki67-positive cell ratio in lung and liver (Figs. 8B–D). However, no such effect was seen in the mice with normal MCF-7 cells which express little β2-AR (Fig. S11). These results indicated that BA restrained chronic stress-mediated breast cancer metastasis via inhibiting β2-AR activation *in vivo*.

3.8. BA suppressed EMT in chronic stress-induced breast cancer metastasis in vivo via the β2-AR-cAMP-PKA-FAK pathway

We further explored the mechanism underlying BA alleviating chronic stress-induced breast cancer metastasis *in vivo*. As confirmed *in vitro*, IHC analysis showed that both the upregulation of N-cadherin, a mesenchymal marker, and MMP2, and down-regulation of E-cadherin, an epithelial marker, induced by CUMS was rescued by the treatment of BA (Figs. 9A and B).

Previous study showed that FAK activation could induce an invasive phenotype of cancer via the β2-AR-cAMP-PKA signaling pathway during depression [10]. The underlying mechanism indicates that the β2-AR-dependent activation of SRC directed FAK phosphorylation and further tumorigenesis [35,36]. We wondered whether the suppression of EMT process by the treatment of BA is associated with the deactivation of SRC and FAK phosphorylation in breast cancer. As expected, the expression of p-SRC, and the downstream effectors p-FAK and p-PXN were significantly decreased with co-treatment of BA in the chronic stress-induced breast cancer metastasis mice model (Figs. 9C and D, and S12A and B). β-AR agonists and CRS-mediated increase of p-SRC, p-FAK and p-PXN was also abolished by BA treatment (Figs. 9E and F). The repeated assay in β2-AR-null MDA-MB-231 cells showed negative results on these biomarkers (Fig. S12C). Notably, H89, an inhibitor of PKA, was also found to block the EMT process and FAK activation induced by β2-AR (Fig. S12D). Therefore, our results demonstrate that BA inhibited chronic stress-induced EMT and metastasis of breast cancer by inhibiting the cAMP-PKA-FAK pathway.

4. Discussion

Studies conducted on both animals and humans have shown that chronic stress is associated with the advancement of preexisting breast cancer [37,38]. Although few consistent relationships between stress and the initial incidence of breast cancer have been found [39,40], metastasis induced by stress was principally presented with growth of evidences. The primary contributor was attributed to the activation of β2-AR and to a lesser degree by HPA axis [41]. By focusing on β2-AR signaling pathway, our results observed that the expression level of β2-AR harmonized with metastatic potency and overexpression/knockout of β2-AR render to/deprive of the invasive ability of breast cancer cell. Meanwhile, the growth of primary tumors did not show any notable effect following the activation of β2-AR induced by stress. To find an alternative therapy from natural product library, our results showed that BA led to a significant decrease of stress-induced breast cancer metastasis in response to β2-AR stimulation, but it had limited impact on breast cancer metastasis in the absence of

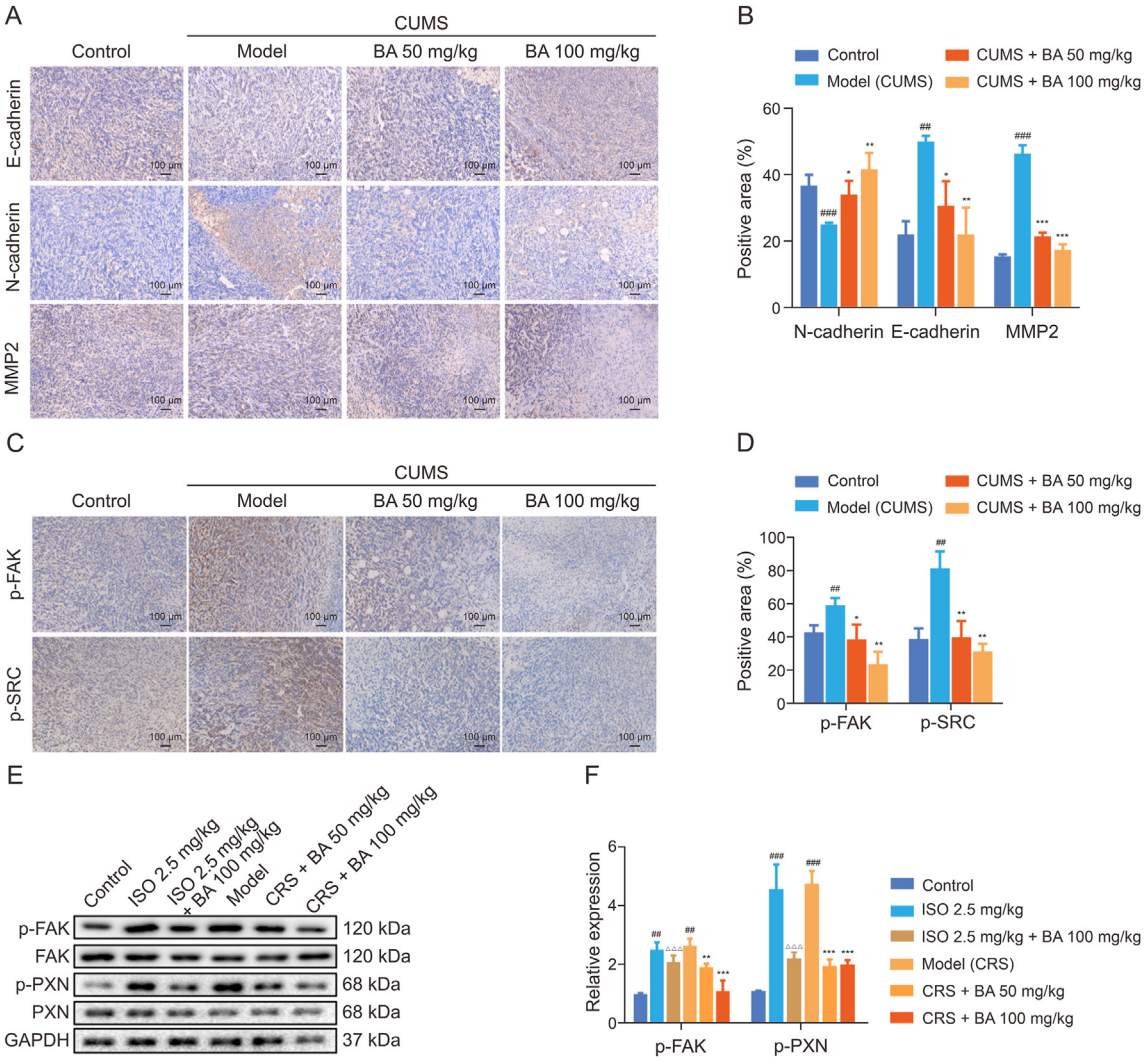

Fig. 9. Baicalin (BA) suppressed epithelial-mesenchymal transition (EMT) in chronic stress-promoted breast cancer metastasis *in vivo* via the β2-adrenergic receptor-cyclic adenosine monophosphate-protein kinase A-focal adhesion kinase (β2-AR-cAMP-PKA-FAK) pathway. (A, B) The ratio of E-cadherin positive, N-cadherin positive, and matrix metalloproteinase 2 (MMP2) positive cells was measured in tumors derived from 4T1 *in situ* chronic unpredictable mild stress (CUMS) tumor model in the presence or the absence of BA by immunohistochemistry (IHC) analysis (A) and quantified (B). (C, D) The ratio of p-FAK positive and p-SRC positive cells was measured in tumors derived from 4T1 *in situ* CUMS tumor model with or without BA treatment by IHC analysis (C) and quantified (D). $n = 6$. (E , F) p-FAK and p-PXN levels were examined in *in situ* tumors derived from 4T1 cells treated with isoprenaline (ISO) plus BA or not, and chronic restraint stress (CRS model) of 4T1 cells treated with different concentrations of BA (E), and quantified (F). $n = 3$. $^{\#\#}P < 0.01$, $^{\#\#\#}P < 0.001$ vs. control; $^{*}P < 0.05$, $^{**}P < 0.01$, $^{***}P < 0.01$ vs model; $^{\triangle\triangle\triangle}P < 0.001$ vs. ISO. GAPDH: glyceraldehyde-3-phosphate dehydrogenase.

stress. To our knowledge, this is the first study revealing BA's role against chronic stress-induced breast cancer metastasis.

It was reported that β1/2AR-blocker propranolol has been clinically studied in the prevention of breast cancer metastasis [13]. And our study also demonstrated that propranolol exhibited inhibitory effect on Epi -caused metastasis of breast cancer cells (Fig. S13), which was similar with BA. However, the side effects of non-selective blocker may result in cardiac disorders, rash, fatigue and vitiligo in long-term use [42]. Our results revealed that BA blocked β2-AR activation by binding to allosteric sites of Phe193 and Phe289. The binding pocket is distinct from the position binding with endogenous β2-AR agonists NE and Epi. Further study confirmed that BA inhibited β2-AR function in a noncompetitive manner with a negligible influence on the intrinsic activity of β2-AR. More importantly, we mechanistically verified that the cAMP-PKA-FAK pathway, the downstream signaling pathway of β2-AR, is indeed responsible for β2-AR-mediated inhibition on chronic stress-induced metastasis. These findings suggest a possible design of new selective β2-AR blocker and the underlying mechanism that could be adopted in the medicinal evaluation of the blocker.

Scutellaria baicalensis Georgi is one of the most well-known traditional herbs in Chinese medicine and popularly applied in China for 2000 years. Recent clinical trials with PHY906 (a four-herb traditional decoction containing *Scutellaria baicalensis* Georgi) have proved to increase life span of patients and the therapeutic index of primary cancer treatments, such as chemotherapy and radiation [43,44]. BA, the most abundant and main bioactive constituent, has been pharmacologically studied and found several direct targets in multiple diseases including cancer. For instance, Huang L et al. [45] confirmed that BA could relieve neuropathic pain by regulating α_2-adrenoceptor levels in rats following spinal nerve injury. Cai R et al. [46] found that BA could block colon cancer cell cycle and inhibits cell proliferation by targeting CDK16. In addition, it was reported that BA could induce cellular senescence in human colon cancer cells via upregulation of DEPP [47]. However, these studies focused on either tumor cells or nerves alone, the effect of

BA on stress-induced breast cancer metastasis has not been concerned. The present study revealed that BA exerts a protective effect against chronic stress-promoted breast cancer metastasis via directly binding to β2-AR and antagonized the activation of β2-AR on tumors. Previous study also reported that BA displayed antidepressant effect through reducing serum corticosterone level in mice model [48], which may contribute to delay stress-induced cancer metastasis [49]. Besides β2-AR, several other proteins (LMW-PTP, PKB, APEN, CYCS, and MAPK1) have also been identified in our DARTS and LC-MS/MS assay, among which MAPK1, APEN and PKB have been previously found to be involved in the suppression on tumor [50–52]. It needs further investigation whether these targets are engaged in cancer metastasis in the context of chronic stress. The good news is BA showed good biocompatibility up to 100 mg/kg group in our present study as also reported in previous studies [53]. Considering the herbal extracts of *Scutellaria baicalensis* Georgi have little safety concerns aroused in ancient and contemporary medicinal practice, we believe that BA may have been a new natural candidate for the co-treatment of chronic stress-induced breast cancer metastasis.

5. Conclusions

Taken together, these discoveries emphasize the role of stress in the advancement of cancer and suggest that BA may serve as a new complementary approach to reduce the spread of breast cancer caused by chronic stress. Additionally, this study provides a novel perspective for exploring β2-AR antagonist without the structure of β-Amino alcohol.

CRediT author statement

Qi Jia: Investigation, Methodology, Data curation, Formal analysis; **Yinyin Zhou** and **Li Song**: Formal analysis, Investigation, Methodology, Writing - Original draft preparation; **Ximeng Shi**: Investigation, Methodology, Formal analysis; **Xuan Jiang**: Investigation, Methodology; **Ruizhi Tao**: Methodology, Investigation; **Aiyun Wang**: Supervision, Resources; **Yuanyuan Wu**: Methodology, Validation, Resources; **Zhonghong Wei**: Methodology, Resources; **Yinan Zhang**: Methodology, Formal analysis, Validation, Writing - Reviewing and Editing; **Xiaoman Li**: Conceptualization, Data curation, Resources, Writing - Original draft preparation, and Reviewing and Editing; **Yin Lu**: Conceptualization, Resources, Supervision, Project administration.

Declaration of competing interest

The authors declare that there are no conflicts of interest.

Acknowledgments

This work was supported by the Matching Grant of National Natural Science Foundation of China from Nanjing University of Chinese Medicine (Grant Nos.: NZY81903857, and NZY81703765), the National Natural Science Foundation of China (Grant No.: 21877062), the Opening Project of Chinese Materia Medica First-Class Discipline of Nanjing University of Chinese Medicine (Grant No.: 2020YLXK020), and Postgraduate Research & Practice Innovation Program of Jiangsu Province (Grant Nos.: SJCX21_0707, KYCX21_1772, and KYCX22_2039). We thank the Experiment Center for Science and Technology, Nanjing University of Chinese Medicine for valuable help in the experiment.

Appendix A. Supplementary data

Supplementary data to this article can be found online at https://doi.org/10.1016/j.jpha.2024.01.002.

References

[1] H. Sung, J. Ferlay, R.L. Siegel, et al., Global cancer statistics 2020: GLOBOCAN estimates of incidence and mortality worldwide for 36 cancers in 185 countries, CA Cancer J. Clin. 71 (2021) 209–249.
[2] R.L. Siegel, K.D. Miller, H.E. Fuchs, et al., Cancer statistics, 2021, CA Cancer J. Clin. 71 (2021) 7–33.
[3] Y. Cai, Z. Shao, K. Yu, Determining the optimal (neo)adjuvant regimen for human epidermal growth factor receptor 2-positive breast cancer regarding survival outcome: A network meta-analysis, Front. Immunol. 13 (2022), 919369.
[4] Y. Liang, H. Zhang, X. Song, et al., Metastatic heterogeneity of breast cancer: Molecular mechanism and potential therapeutic targets, Semin. Cancer Biol. 60 (2020) 14–27.
[5] B. Mravec, M. Tibensky, L. Horvathova, Stress and cancer. Part I: Mechanisms mediating the effect of stressors on cancer, J. Neuroimmunol. 346 (2020), 577311.
[6] A. Eckerling, I. Ricon-Becker, L. Sorski, et al., Stress and cancer: Mechanisms, significance and future directions, Nat. Rev. Cancer 21 (2021) 767–785.
[7] T.I. Barron, R.M. Connolly, L. Sharp, et al., Beta blockers and breast cancer mortality: A population- based study, J. Clin. Oncol. 29 (2011) 2635–2644.
[8] R. Gosain, E. Gage-Bouchard, C. Ambrosone, et al., Stress reduction strategies in breast cancer: Review of pharmacologic and non-pharmacologic based strategies, Semin. Immunopathol. 42 (2020) 719–734.
[9] B.W. Renz, R. Takahashi, T. Tanaka, et al., β2 adrenergic-neurotrophin feedforward loop promotes pancreatic cancer, Cancer Cell 34 (2018) 863–867.
[10] Y. Cheng, X. Gao, X. Li, et al., Depression promotes prostate cancer invasion and metastasis via a sympathetic-cAMP-FAK signaling pathway, Oncogene 37 (2018) 2953–2966.
[11] J.G. Hiller, S.W. Cole, E.M. Crone, et al., Preoperative β-blockade with propranolol reduces biomarkers of metastasis in breast cancer: A phase II randomized trial, Clin. Cancer Res. 26 (2020) 1803–1811.
[12] B. Mravec, M. Tibensky, L. Horvathova, Stress and cancer. Part II: Therapeutic implications for oncology, J. Neuroimmunol. 346 (2020), 577312.
[13] L. Shaashua, M. Shabat-Simon, R. Haldar, et al., Perioperative COX-2 and β-adrenergic blockade improves metastatic biomarkers in breast cancer patients in a phase-II randomized trial, Clin. Cancer Res. 23 (2017) 4651–4661.
[14] M.B. Hopson, S. Lee, M. Accordino, et al., Phase II study of propranolol feasibility with neoadjuvant chemotherapy in patients with newly diagnosed breast cancer, Breast Cancer Res. Treat. 188 (2021) 427–432.
[15] D.J. Newman, G.M. Cragg, Natural products as sources of new drugs over the nearly four decades from 01/1981 to 09/2019, J. Nat. Prod. 83 (2020) 770–803.
[16] C. Qian, C. Yang, Y. Tang, et al., Pharmacological manipulation of Ezh2 with salvianolic acid B results in tumor vascular normalization and synergizes with cisplatin and T cell-mediated immunotherapy, Pharmacol. Res. 182 (2022), 106333.
[17] X. Li, Q. Jia, Y. Zhou, et al., Tanshinone IIA attenuates the stemness of breast cancer cells via targeting the miR-125b/STARD13 axis, Exp. Hematol. Oncol. 11 (2022), 2.
[18] J. Wang, S. Wang, S. Liu, et al., Molecular mechanism of Bupleuri *Radix* and Scutellariae *Radix* drug pair for depression based on integrative pharmacology platform of traditional Chinese medicine, China J. Chin. Mater. Med. 43 (2018) 1323–1330.
[19] T. Zhao, H. Tang, L. Xie, et al., *Scutellaria baicalensis* Georgi. (Lamiaceae): A review of its traditional uses, botany, phytochemistry, pharmacology and toxicology, J Pharm. Pharmacol. 71 (2019) 1353–1369.
[20] S. Singh, A. Meena, S. Luqman, Baicalin mediated regulation of key signaling pathways in cancer, Pharmacol. Res. 164 (2021), 105387.
[21] Z. Xiao, Z. Cao, J. Yang, et al., Baicalin promotes hippocampal neurogenesis via the Wnt/β-catenin pathway in a chronic unpredictable mild stress-induced mouse model of depression, Biochem. Pharmacol. 190 (2021), 114594.
[22] K. Liu, L. Guo, Y. Guo, et al., AEG-1 3'-untranslated region functions as a ceRNA in inducing epithelial-mesenchymal transition of human non-small cell lung cancer by regulating miR-30a activity, Eur. J. Cell Biol. 94 (2015) 22–31.
[23] C. Zhang, M. Cui, Y. Cui, et al., A Semi-Quantitative Drug Affinity Responsive Target Stability (DARTS) assay for studying Rapamycin/mTOR interaction, J. Vis. Exp. (2019), 150.
[24] J.R. Wiśniewski, A. Zougman, N. Nagaraj, et al., Universal sample preparation method for proteome analysis, Nat. Meth. 6 (2009) 359–362.
[25] E. Weerapana, A.E. Speers, B.F. Cravatt, Tandem orthogonal proteolysis-activity-based protein profiling (TOP-ABPP)—a general method for mapping sites of probe modification in proteomes, Nat. Protoc. 2 (2007) 1414–1425.
[26] R. Jafari, H. Almqvist, H. Axelsson, et al., The cellular thermal shift assay for evaluating drug target interactions in cells, Nat. Protoc. 9 (2014) 2100–2122.
[27] P. Kleiner, W. Heydenreuter, M. Stahl, et al., A whole proteome inventory of background photocrosslinker binding, Angew. Chem. Int. Ed. Engl. 56 (2017) 1396–1401.

[28] K. Hayakawa, M. Yodo, S. Ohsuki, et al., Novel bicycloannulation via tandem vinylation and intramolecular Diels-Alder reaction of five-membered heterocycles: A new approach to construction of psoralen and azapsoralen, J. Am. Chem. Soc. 106 (1984) 6735–6740.
[29] M. Walko, E. Hewitt, S.E. Radford, et al., Design and synthesis of cysteine-specific labels for photo-crosslinking studies, RSC Adv. 9 (2019) 7610–7614.
[30] K. Cheng, J.S. Lee, P. Hao, et al., Tetrazole-based probes for integrated phenotypic screening, affinity-based proteome profiling, and sensitive detection of a cancer biomarker, Angew. Chem. Int. Ed. Engl. 56 (2017) 15044–15048.
[31] L. Liao, X. Song, L. Wang, et al., Highly selective inhibition of IMPDH2 provides the basis of antineuroinflammation therapy, Proc. Natl. Acad. Sci. U. S. A. 114 (2017) E5986–e5994.
[32] X. Zheng, Y. Pan, G. Yang, et al., Kaempferol impairs aerobic glycolysis against melanoma metastasis via inhibiting the mitochondrial binding of HK2 and VDAC1, Eur. J. Pharmacol. 931 (2022), 175226.
[33] B. Zhang, S. Ma, I. Rachmin, et al., Hyperactivation of sympathetic nerves drives depletion of melanocyte stem cells, Nature 577 (2020) 676–681.
[34] Target identification using drug affinity responsive target stability (DARTS), Sci. Bus. eXchange 3 (2010), 71.
[35] A.K. Sood, G.N. Armaiz-Pena, J. Halder, et al., Adrenergic modulation of focal adhesion kinase protects human ovarian cancer cells from anoikis, J. Clin. Invest. 120 (2010) 1515–1523.
[36] A.G. Beristain, S.D. Molyneux, P.A. Joshi, et al., PKA signaling drives mammary tumorigenesis through Src, Oncogene 34 (2015) 1160–1173.
[37] E.K. Sloan, S.J. Priceman, B.F. Cox, et al., The sympathetic nervous system induces a metastatic switch in primary breast cancer, Cancer Res. 70 (2010) 7042–7052.
[38] P. Du, H. Zeng, Y. Xiao, et al., Chronic stress promotes EMT-mediated metastasis through activation of STAT3 signaling pathway by miR-337-3p in breast cancer, Cell Death Dis. 11 (2020), 761.
[39] M.A. Pereira, A. Araújo, M. Simões, et al., Influence of psychological factors in breast and lung cancer risk–A systematic review, Front. Psychol. 12 (2022), 769394.
[40] M.J. Schoemaker, M.E. Jones, L.B. Wright, et al., Psychological stress, adverse life events and breast cancer incidence: A cohort investigation in 106, 000 women in the United Kingdom, Breast Cancer Res. 18 (2016), 72.
[41] E. Rosenne, L. Sorski, L. Shaashua, et al., *In vivo* suppression of NK cell cytotoxicity by stress and surgery: Glucocorticoids have a minor role compared to catecholamines and prostaglandins, Brain Behav. Immun. 37 (2014) 207–219.
[42] S. Gandhi, M.R. Pandey, K. Attwood, et al., Phase I clinical trial of combination propranolol and pembrolizumab in locally advanced and metastatic melanoma: Safety, tolerability, and preliminary evidence of antitumor activity, Clin. Cancer Res. 27 (2021) 87–95.
[43] C.A. Changou, H.S. Shiah, L.T. Chen, et al., A phase II clinical trial on the combination therapy of PHY906 plus capecitabine in hepatocellular carcinoma, Oncol. 26 (2021) e367–e373.
[44] S.H. Liu, Y.C. Cheng, Old formula, new Rx: The journey of PHY906 as cancer adjuvant therapy, J. Ethnopharmacol. 140 (2012) 614–623.
[45] L. Huang, S. Jia, X. Sun, et al., Baicalin relieves neuropathic pain by regulating α2-adrenoceptor levels in rats following spinal nerve injury, Exp. Ther. Med. 20 (2020) 2684–2690.
[46] R. Cai, Y.P. Zhou, Y.H. Li, et al., Baicalin blocks colon cancer cell cycle and inhibits cell proliferation through miR-139-3p upregulation by targeting CDK16, Am. J. Chin. Med. 51 (2023) 189–203.
[47] Z. Wang, L. Ma, M. Su, et al., Baicalin induces cellular senescence in human colon cancer cells via upregulation of DEPP and the activation of Ras/Raf/MEK/ERK signaling, Cell Death Dis. 9 (2018), 217.
[48] K. Zhang, M. He, F. Wang, et al., Revealing antidepressant mechanisms of baicalin in hypothalamus through systems approaches in corticosterone-induced depressed mice, Neurosci. 13 (2019), 834.
[49] H. Yang, L. Xia, J. Chen, et al., Stress–glucocorticoid–TSC22D3 axis compromises therapy-induced antitumor immunity, Nat. Med. 25 (2019) 1428–1441.
[50] R. Deng, H.L. Zhang, J.H. Huang, et al., MAPK1/3 kinase-dependent ULK1 degradation attenuates mitophagy and promotes breast cancer bone metastasis, Autophagy 17 (2021) 3011–3029.
[51] T. Huang, Y. Wang, M. Huang, et al., LINC00470 accelerates the proliferation and metastasis of melanoma through promoting APEX1 expression, Cell Death Dis. 12 (2021), 410.
[52] J. Chen, C.B. Yuan, B. Yang, et al., Baicalin inhibits EMT through PDK1/AKT signaling in human nonsmall cell lung cancer, J. Oncol. 2021 (2021), 4391581.
[53] M. Li, A. Shi, H. Pang, et al., Safety, tolerability, and pharmacokinetics of a single ascending dose of baicalein chewable tablets in healthy subjects, J. Ethnopharmacol. 156 (2014) 210–215.